iScience

CellPress
OPEN ACCESS

Article

Myeloid TLR4 signaling promotes post-injury withdrawal resolution of murine liver fibrosis

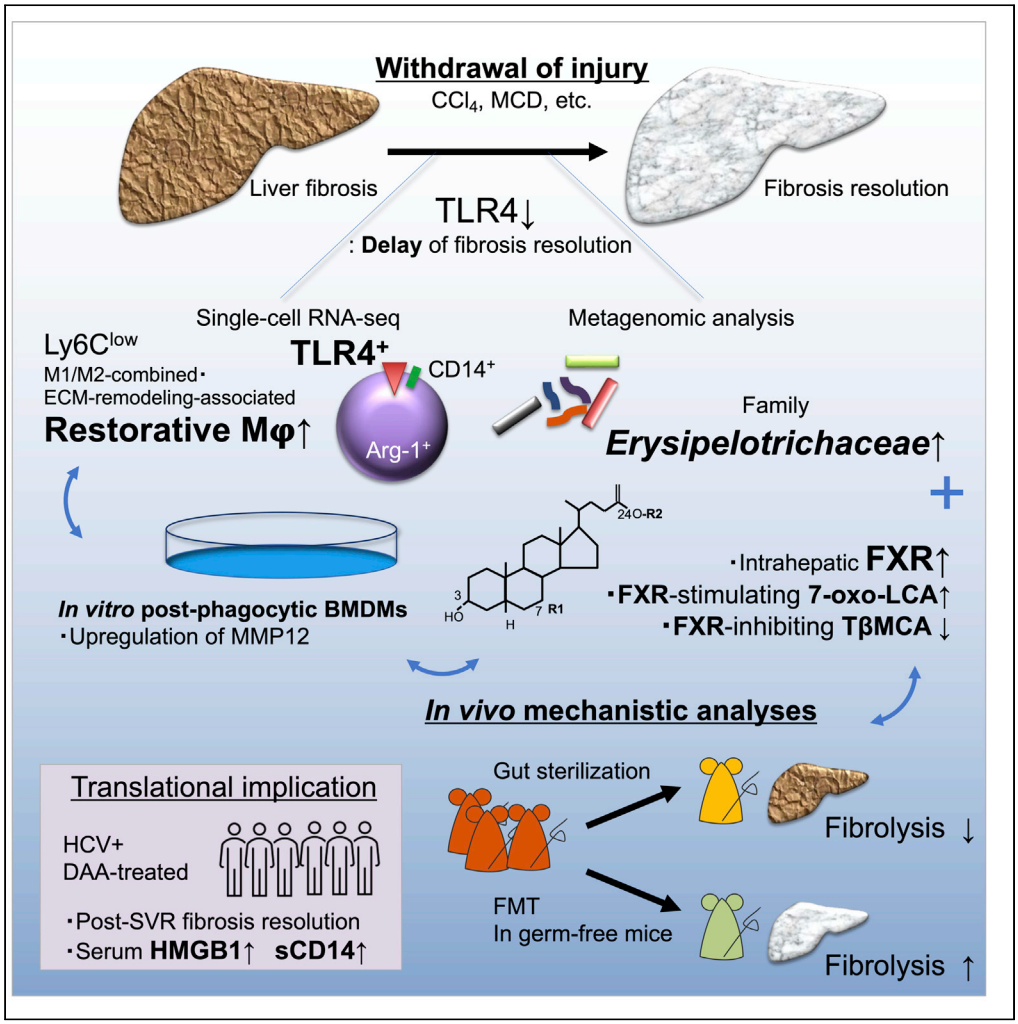

Yoichi Takimoto, Po-sung Chu, Nobuhiro Nakamoto, ..., Masataka Ichikawa, Akira Honda, Takanori Kanai

pschu0928@icloud.com (P.-s.C.)
takagast@z2.keio.jp (T.K.)

Highlights

TLR4 inhibition *in vivo* delays post-injury withdrawal liver fibrosis resolution

Tlr4-expressing myeloid cells with restorative features accumulate upon resolution

Enrichment of family Erysipelotrichaceae links to FXR-acting bile acids

TLR4 and bile acid-FXR axis synergistically upregulate MMP12 *in vitro*

Takimoto et al., iScience *26*, 106220
March 17, 2023
https://doi.org/10.1016/j.isci.2023.106220

iScience

CellPress
OPEN ACCESS

Article

Myeloid TLR4 signaling promotes post-injury withdrawal resolution of murine liver fibrosis

Yoichi Takimoto,[1] Po-sung Chu,[1,*] Nobuhiro Nakamoto,[1] Yuya Hagihara,[1] Yohei Mikami,[1] Kentaro Miyamoto,[1,2] Rei Morikawa,[1] Toshiaki Teratani,[1] Nobuhito Taniki,[1] Sota Fujimori,[1,3] Takahiro Suzuki,[1,2] Yuzo Koda,[1,3] Rino Ishihara,[1] Masataka Ichikawa,[1] Akira Honda,[4] and Takanori Kanai[1,5,*]

SUMMARY

The fate of resolution of liver fibrosis after withdrawal of liver injury is still incompletely elucidated. Toll-like receptor 4 (TLR4) in tissue fibroblasts is pro-fibrogenic. After withdrawal of liver injury, we unexpectedly observed a significant delay of fibrosis resolution as TLR4 signaling was pharmacologically inhibited *in vivo* in two murine models. Single-cell transcriptome analysis of hepatic CD11b$^+$ cells, main producers of matrix metalloproteinases (MMPs), revealed a prominent cluster of restorative *Tlr4*-expressing *Ly6c2*-low myeloid cells. Delayed resolution after gut sterilization suggested its microbiome-dependent nature. Enrichment of a metabolic pathway linking to a significant increase of bile salt hydrolase-possessing family Erysipelotrichaceae during resolution. Farnesoid X receptor-stimulating secondary bile acids including 7-oxo-lithocholic acids upregulated MMP12 and TLR4 in myeloid cells *in vitro*. Fecal material transplant in germ-free mice confirmed phenotypical correlations *in vivo*. These findings highlight a pro-fibrolytic role of myeloid TLR4 signaling after injury withdrawal and may provide targets for anti-fibrotic therapy.

INTRODUCTION

Wound healing, a highly conserved protective response to tissue injury, may culminate in tissue fibrosis and organ failure if homeostasis is disrupted. Liver cirrhosis, a common pathological feature associated with persistent liver injury, results from uncontrolled fibrogenesis and ineffective fibrosis resolution.[1] Successful suppression of hepatitis B virus (HBV), eradication of hepatitis C virus (HCV), and lifestyle modifications for non-alcoholic steatohepatitis (NASH) can reverse liver fibrosis.[2–4] The liver has provided the most cogent evidence of the bidirectionality of organ fibrosis.[1] However, liver fibrosis regression has been observed in some, but not all, patients with chronic hepatitis C (CHC) after HCV eradication.[5,6] Our knowledge of unsuccessful fibrosis resolution in some patients is still incomplete. What controls the fate of fibrosis regression after withdrawal of liver injury is still mostly unknown; its clarification provides translational significance.

Previous studies have focused on hepatic stellate cells (HSCs), which are the primary extracellular matrix (ECM)-producing fibroblasts, and their crosstalk with inflammatory cells during liver fibrogenesis.[7] During the process of fibrosis resolution after injury withdrawal, pro-fibrolytic macrophages are spotlighted.[5] Ramachandran et al. identified a group of recruited "restorative macrophages" responsible for tissue remodeling and characterized them with a low expression of lymphocyte antigen 6 complex, locus C1 (Ly6C) with the tractable carbon tetrachloride (CCl_4)-induced model of reversible liver fibrosis.[8] The transfer of bone marrow (BM)-derived cells, including monocytes/macrophages or M1 polarized macrophages, promotes liver fibrosis resolution.[9,10] However, the precise mechanism of how and to what extent liver fibrosis is resolved after persistent liver injury ceases is still not fully elucidated.

The liver is constantly exposed to immunogenic stimuli via pathogen-derived molecules due to a unique circulation pathway from the gut. Pattern recognition receptors for pathogen- or damage-associated molecular patterns (PAMPs or DAMPs) in the liver have also been examined in hepatic tolerance,[11] inflammation, and fibrogenesis.[12] Among them, the "gut microbiota–lipopolysaccharide (LPS)–toll-like receptor 4 (TLR4) axis" is one of the most studied pro-fibrogenic pathways. TLR4 has demonstrated fibrosis-promoting features via HSC, Kupffer cell, or liver sinusoidal endothelial cell activation that has been proven by

[1]Division of Gastroenterology and Hepatology, Department of Internal Medicine, Keio University School of Medicine, 35 Shinanomachi, Shinjuku-ku, Tokyo 160-8582, Japan

[2]Miyarisan Pharmaceutical Co., Ltd, Kita-ku, Tokyo 114-0016, Japan

[3]Research Unit/Immunology and Inflammation, Sohyaku Innovative Research Division, Mitsubishi Tanabe Pharma Corporation, Yokohama, Kanagawa 227-0033, Japan

[4]Division of Gastroenterology and Hepatology, Department of Internal Medicine, Tokyo Medical University Ibaraki Medical Center, Inashiki-gun, Ibaraki 300-0395, Japan

[5]Lead contact

*Correspondence: pschu0928@icloud.com (P.-s.C.), takagast@z2.keio.jp (T.K.)

https://doi.org/10.1016/j.isci.2023.106220

genetic ablation and gut sterilization in various murine models of liver fibrosis.[7,13] However, some studies have demonstrated conflicting phenotypes associated with this pro-fibrogenic axis[14–16] in models with chronic liver injury. Mazagova and Wang et al. showed that the commensal microbiota prevented, rather than promoted, liver fibrosis in a CCl_4-induced liver fibrosis model developed in germ-free mice.[15] Moreover, although bile acids (BA) and their receptors, such as the farnesoid X receptor (FXR), have been targeted for hepatic inflammation, fibrosis, and regeneration,[17] their roles in fibrosis resolution and interaction between restorative macrophages are still ill-defined.

By pharmacological inhibition of TLR4 signaling *in vivo* with TAK-242, we demonstrated unexpected delay, rather than promotion, of fibrosis resolution in two murine models of post-injury withdrawal fibrosis resolution. Specific metagenomic alterations and changes in BA metabolism via FXR signaling in restorative macrophages were also unraveled.

RESULTS

Pharmacological inhibition of TLR4 signaling with TAK-242 significantly delays post injury-withdrawal liver fibrosis resolution *in vivo*

To know whether TLR4 signaling influence post-injury withdrawal liver fibrosis resolution, a well-established and highly tractable CCl_4-induced murine liver fibrosis resolution model[8] was utilized. The development and reversal of liver fibrosis were confirmed (Figures S1A and S1B). Serum ALT levels, representative of liver injury, peaked at 24 h after the last injection of CCl_4 (Figure S1C, left). ECM accumulation peaked at 48 h (Figure S1C, middle and right).

TAK-242, a TLR4 antagonist, binds to the intracellular toll/interleukin-1 receptor (TIR) domain and inhibits TLR4 signaling.[18] We examined whether pharmacological inhibition of TLR4 signaling with TAK-242 at the peak of ECM accumulation (e.g., at 48 h) influences post-injury withdrawal liver fibrosis resolution or not (Figure 1A). Contrary to previously known pro-fibrogenic roles of TLR4, the intrahepatic accumulation of ECM, assessed by histological analyses and intrahepatic hydroxyproline levels, was unexpectedly significantly higher at 96 h, indicating delay, rather than promotion, of liver fibrosis resolution, without a significant change of ALT (Figures 1B–1E) by TAK-242.

Such higher levels ECM accumulation observed at 96 h in mice treated with TAK-242 could hardly result from an increase in the activation of fibrogenesis, as we observed that expression of intrahepatic fibrogenesis markers, primarily produced by the activated HSCs, was downregulated by TAK-242 (Figure 1F). Significant downregulation of hepatic MMP12, but not MMP9 or MMP13, following administration of TAK-242, was observed (Figure 1G). Hence, downregulation of MMP12 may account for this delay.

During usual fibrosis resolution, expression of HSC fibrosis markers decreased gradually (Figure S1D), while hepatic expression of *Tlr4* (but not *Tlr2*, *Tlr6* or *Tlr9*) and *Mmp12* (but not *Mmp9* or *Mmp13*) increased during resolution, despite of some chronological variations (Figure S1E). Of note, as liver fibrosis resolution proceeded, HMGB1, an endogenous TLR4 ligand classified as damage-associated molecular pattern (DAMP) molecule, was also gradually upregulated in the whole liver (Figure S1F). These results implicated possible existence of a functional TLR4 signaling circuit during post-injury withdrawal fibrosis resolution.

We confirmed the findings with a second murine model of diet-induced fibrosis resolution, as shown in Figure S1G. Wild-type mice were fed with methionine and choline deficient (MCD) diets for 5 weeks to induce steatohepatitis. The diets were then switched to normal diet (ND) for 10 days to induce post-injury withdrawal spontaneous resolution (MCD/ND model). Significantly higher hepatic *Tlr4* expression compared to that of mice fed with normal chow, was observed during resolution (Figure S1H). Spontaneous resolution of hepatocyte injury, along with disease activity of steatohepatitis was observed; however, TAK-242 administration significantly delayed the resolution of liver fibrosis (Figures S2J–S2M). Significantly lower hepatic expression of *Mmp12* in the TAK-242 group was also confirmed in this model (Figure S1N).

During usual fibrosis resolution, intrahepatic $CD11b^+$ macrophages accumulated (Figures S2A and S2B) and showed differential Ly6C expression and intrahepatic frequencies (Figure S2C), as previously reported.[8] Persistently higher frequency of intrahepatic $Ly6c^{low}$ $CD11b^+$ macrophages in MCD diet-fed mice undergone 10-14 days of resolution was also confirmed (Figure S1I). $Ly6C^{low}$ macrophages demonstrated increased CD11c and CX3CR1 expression during resolution (Figure S2D). By using a pan-MMP substrate (MMPsense)

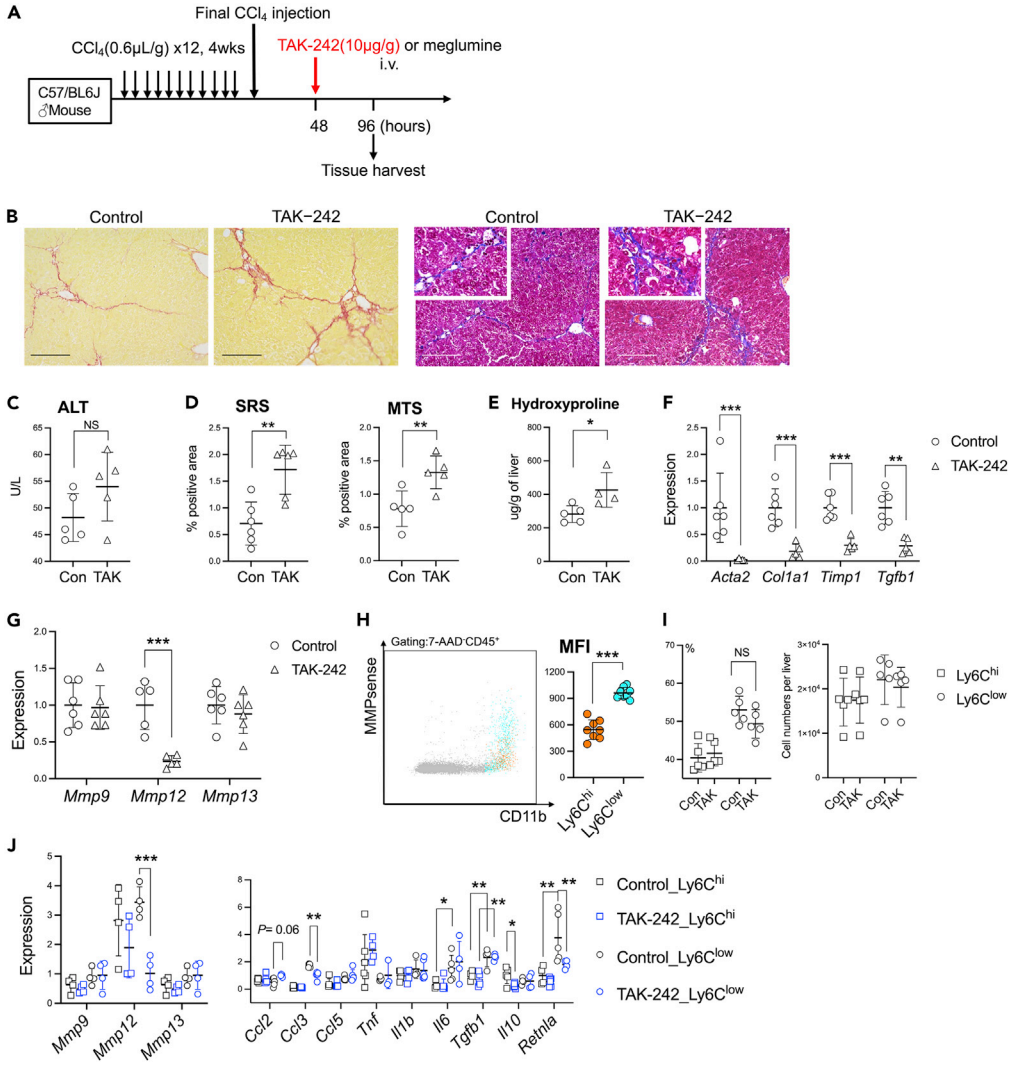

Figure 1. Pharmacological TLR4 inhibition by TAK-242 delays CCl_4-induced liver fibrosis resolution

(A) Schematic representation.

(B) Representative hepatic photomicrographs of sirius red (left), Masson trichrome (right)−stained sections, accompanied with a 4-time magnification demonstrating portal to portal areas. A scale bar represents 500 μm.

(C) Serum ALT levels (n = 5–6).

(D) Quantification of stained areas observed with sirius red staining (SRS) and Masson trichrome staining (MTS) by morphometric pixel analyses (n = 5–6).

(E) Hepatic hydroxyproline content (n = 4–5).

(F and G) Quantitative RT-PCR analysis of featured genes of the livers relative to control group (n = 4–5).

(H) A representative of CD11b and MMPsense staining by flow cytometry at 96 h. Mean fluorescence intensity (MFI) of MMPsense is represented by Ly6C levels. (n = 7–8).

(I) Intrahepatic percentages (left) and cell numbers (per liver; right) of $Ly6C^{hi}$ or $Ly6C^{low}$ among $CD11b^+$ macrophages (n = 5).

(J) Quantitative RT-PCR analysis of featured genes of flow cytometry-sorted intrahepatic $Ly6C^{hi}$ or $Ly6C^{low}$ $CD11b^+$ macrophages relative to TAK-242-treated $Ly6C^{low}$ $CD11b^+$ macrophages (closed squares, n = 4–5). Con, control; TAK, TAK-242. Data show the mean ± SD. *p < 0.05, **p < 0.01, ***p < 0.001, unless otherwise specified. NS, not significant. See also Figures S1 and S2.

that emits fluorescence after cleavage by MMP *in vivo*, we demonstrated that intrahepatic $CD11b^+$ cells were principal producers of MMPs (Figure 1H, left). $Ly6C^{low}$ $CD11b^+$ cells expressed significantly higher levels of MMPs than $Ly6C^{hi}$ cells (Figure 1H, right). Intrahepatic frequencies of other principal immune cells are shown in Figure S2E. Pharmacological TLR4 inhibition by TAK-242 didn't significantly change the frequencies of Ly6Clow myeloid cells (Figure 1I), however, it downregulated MMP12 and CCL3 and depressed the expression

of *Retnla* in intrahepatic Ly6C^{low} CD11b^{+} macrophages (flow cytometry-sorted, exclusive of CD3e^{+}, CD19^{+} and NK1.1^{+} cells, Figure 1J). Phagocytosis markers like *Cd36* and *Mertk*, were consistently and highly expressed in Ly6C^{low} macrophages; no effect of TAK-242 was observed (Figure S2F).

Single-cell transcriptome analysis defines a distinct cluster of TLR4-upregulated myeloid cells with a scar-resolving phenotype during hepatic fibrosis resolution

Since intrahepatic MMP-producing CD11b^{+} immune cells may account for the delayed resolution after TLR4-signaling inhibition, we performed single-cell RNA sequencing (scRNA-seq) to identify the cellular subset that accounts for liver fibrosis resolution. Hepatic CD11b^{+} nonparenchymal CD45^{+} cells were isolated (Figures 2A and S3A). Uninjured mice (as controls) and mice sacrificed at 96 h after the last CCl_4 were compared due to similar ALT levels (Figure S1C) and intrahepatic CD11b^{+} frequencies (Figure S2B). More than 7,000 cells that met the quality thresholds were analyzed.

The CCl_4-induced liver fibrosis resolution induced qualitative transcriptional differences in CD11b^{+} cell clustering compared to those observed in uninjured controls (Figures 2B and S3C). While clusters 0-1 represented natural killer cells and were excluded from further analysis as shown in the Method, clusters 2-6 represented principal groups of mononuclear phagocytes (MP) were identified, MP (1) to MP (5), as demonstrated by the genes showing significant changes (Figures S3B and S3C). Among the five MP clusters, MP (3), which was hardly detected in the uninjured steady state, increased in mice undergoing liver fibrosis resolution (Figures 2B and 2C). A gene expression heatmap showing an unbiased generation of the top twenty differentially expressed genes for each cluster is presented in Figure 2D. Relatively maintained expression of *Lyz2* implicated their myeloid nature (Figures 2D and S3C). Among the differentially expressed genes, the expression of *Ly6c2* (encoding Ly6C) was high in MP (1) and MP (4); low in MP (2) and MP (3) (Figures 2D, 2E, and S3C). Moreover, only *Ly6c2*-low myeloid cells belonging to MP (3) also demonstrated upregulation of genes involved in ECM remodeling (*Spp1*, *Cd44*, *Fn1*, *Tgm2*),[19] post-phagocytosis (*Trem2*), anti-inflammatory (*Cstb*, *AA467197* known as *Mir-147*[20]) and anti-fibrotic pathways (*Igf1*, *Mif*),[21,22] and combined properties of both M1 (*Cd14*, *Serpine1*) and M2 (*Arg1*, *Ccl9*, *Ccl24*) features (Figures 2D–2F).

Additionally, many of these genes highly expressed in MP (3) were associated with the TLR4 pathway (*Cd14*, *Spp1*, *Mif*, *Cstb*, and *AA467197*; shown in Figures 2D–2F). These scar-resolving transcriptomic features of MP (3) were congruent with previous reports, such as "restorative Ly6C^{low} macrophages",[8] shared in part with CD9^{+}TREM2^{+} "scar-associated macrophages," as Ramanchandran et al. demonstrated that they were circulating monocyte-derived and were pro-fibrogenic, in both cirrhosis in human and CCl_4-induced fibrosis in mice.[23] A combinational analysis of reported gene expression modules inclusive of *Cd9*, *Trem2*, *Spp1*, *Lgals3*, *Ccl2*, *Pdgfb*, *Vegfa*, *Hes1* and *Sell*[23] suggests that MP (2) and MP (3) were monocyte-derived, while *Cd9*$^{+}$*Trem2*$^{+}$*Hes1*$^{+}$*Sell*$^{-}$ MP (3), the only expanding cluster, might be more related with such scar-associating phenotypes than *Cd9*^{dim}*Trem2*$^{-}$*Hes1*$^{+}$*Sell*$^{-}$ MP (2) (Figure 2E). In addition, *Ly6c2*$^{+}$*Ccr2*$^{+}$*Sell*$^{+}$ MP (1) was suggested to be tissue monocytes (Figure 2E), while *Ly6c2*$^{+}$*Ccr2*$^{+}$*Sell*^{dim}*Stat1*$^{+}$ *Ccl2*$^{-}$*Pdgfb*$^{+}$ MP (4), a diminishing cluster, was suggested to be inflammatory tissue monocytes (Figures 2C and 2E). Cells in MP (5) partially expressed, but not co-expressed, *Cd163*, a Kupffer cell marker, and *Ztbt4*, a transcription factor selectively expressed by classical dendritic cells (cDCs) and their committed progenitors,[24] *Clec9a* and *Cd209a*.Therefore, MP (5) was deemed to be a combination of both Kupffer cells and cDCs (Figures 2E and S3C). However, expression patterns of various other KC lineage markers, such as *Nr1h3*[25] (expressed in MP(2)-(5)), along with the very low to non-expression of *Clec4f*, *Marco*, *Vsig4*, and *Cd5l* (Figure S3C), might implicate that the roles of KC may be insufficiently explored due to limitations in CCl_4 model (a KC-depleting model[23]) or in methods of gradient isolation of hepatic mononuclear cells. The lower expression of *Clec10A* in MP (3) compared to MP (5) also helps distinguishing MP (3) from DCs (Figure 2D).[26] MP (1) to MP (5) demonstrated characteristic transcriptional profiles of TLRs (Figure S3D). Upregulation of TLR4 was significantly and exclusively elevated in MP (3). Therefore, we assume that these *Tlr4*-expressing MP (3) myeloid cells were macrophages related to liver fibrosis resolution.

Moreover, with flow cytometric analysis of intrahepatic mononuclear cells of livers harvested in uninjured mice (as controls) and mice sacrificed at 24 or 96 h after the last CCl_4 (as shown in Figure S1A), we demonstrated that TLR4^{+} CD14^{+} Arg-1^{+} Ly6C^{low} CD11b^{+} macrophages increased significantly in the 96 h-group, compared to the 24 h-group (at which liver injury peaks, Figure S1C) and uninjured controls (Figures 2G and 2H). These results showed that CD14^{+} Arg-1^{+} TLR4^{+} macrophages increased from 24 h to 96 h after last CCl_4; they were unlikely to be remnants of inflammatory monocytes accumulated with liver injury.

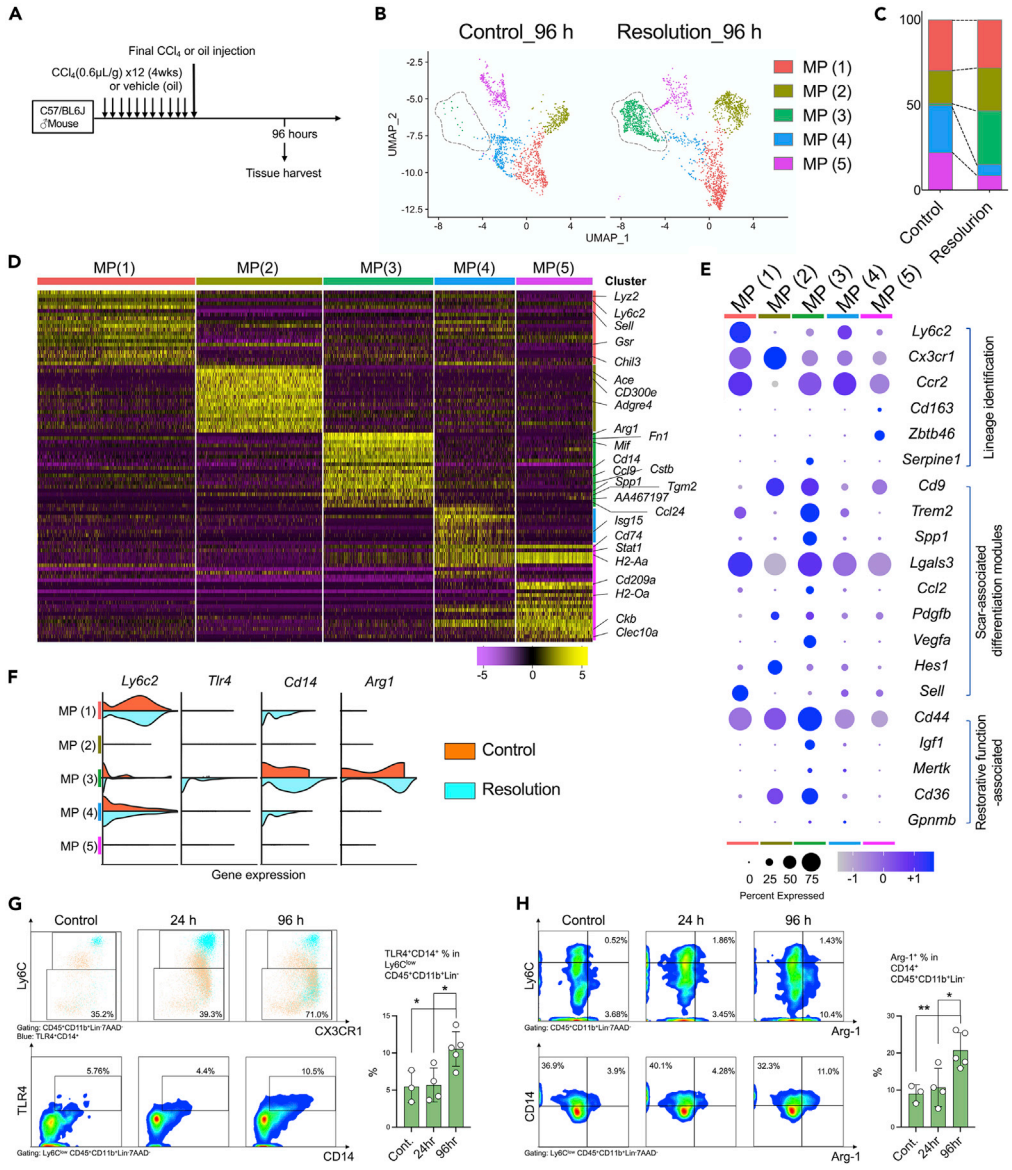

Figure 2. Transcriptional diversity of intrahepatic CD45^{+}CD11b^{+} cells during fibrosis resolution

(A) Schematic representation.

(B) UMAP projections of identified graph-based cell clusters from scRNA-seq data derived from main macrophage segments in hepatic CD45^{+}CD11b^{+} cells. The dashed circle represents MP (3).

(C) Cell proportions of (B).

(D) Heatmaps of normalized and scaled expression of representative marker genes in 5 main clusters of MP cells.

(E) Dot plot of representative gene expression in five major clusters of MP cells. The circle size denotes percentage with expression within each cluster; color (blue, high; light purple, low) denotes normalized expression levels.

(F) Scaled expressions of genes in five major clusters of MP cells compared with those derived during the resolution and the corresponding controls.

(G and H) Flow cytometric analyses of intrahepatic mononuclear cells of uninjured control and mice sacrificed at 24 h or 96 h after last CCl_4 (refer to Figure S1A). MP, mononuclear phagocyte. Data show the mean ± SD. *p < 0.05, **p < 0.01. See also Figure S3.

To demonstrate whether these *Tlr4*-expressing myeloid cells with restorative properties could be observed in progressive liver disease states, we next compared these macrophages observed during post CCl_4 withdrawal liver fibrosis resolution murine model to those observed in a mouse dietary NASH model which were previously reported.[27] Wound-healing Ly6C^{low}-RM (recruited macrophage) highly expressed *Itgam*

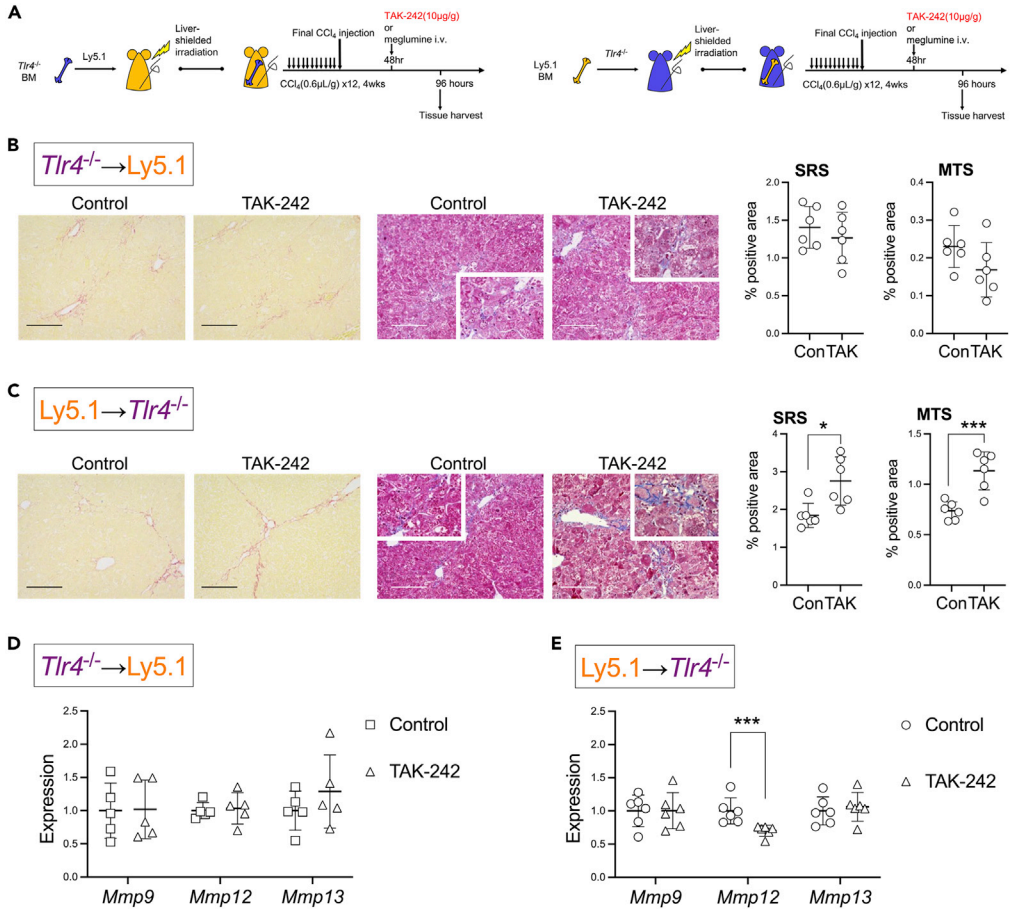

Figure 3. TLR4 signaling in bone marrow-derived cells is crucial for CCl_4-induced liver fibrosis resolution

(A) Schematic representation.

(B and C) Representative hepatic photomicrographs of sirius red (left), Masson trichrome (middle)—stained sections, accompanied with a 4-time magnification demonstrating portal to portal areas. Quantification of stained areas observed by morphometric pixel analyses are shown (n = 6). A scale bar represents 500μm.

(D and E) Quantitative RT-PCR analysis of featured genes of the livers relative to control group (n = 5–6). Con, control; TAK, TAK-242. Data show the mean ± SD. *p < 0.05, ***p < 0.001. See also Figure S4.

(encoding CD11b), *Cx3cr1*, and *Itgax* (encoding CD11c), as shown in Figure S3E. These results are congruent to our key features (Figures 1J and S2D). In addition, when compared with its Ly6C^{hi} counterpart, Ly6C^{low}-RM expressed higher *Tlr4*, *Mmp12*, *Retnla*, *Ccl3* and *AA467197*(*Mir-147*), as shown in Figure S3F. These results are also similar to our key features (Figures 1J and 2), implicating that a TLR4-related ECM-degrading driving force may also simultaneously exist in progressive liver disease states.

TLR4 signaling in the BM-derived cells is crucial for liver fibrosis resolution

To elucidate whether the localization of TLR4 signaling in liver parenchymal or myeloid-derived cells influences liver fibrosis resolution, we applied the CCl_4-induced model of reversible liver fibrosis to BM-transplanted mice (Figure 3A). To avoid the influence of intrahepatic Kupffer cells, we applied a model of liver-shielded irradiation before BM transplantation (BMT). We have confirmed that intrahepatic Kupffer cells were not influenced in our previous report.[28] Successful BM transplantation (BMT) was confirmed, as shown in Figure S4A. In WT mice transplanted with *Tlr4*$^{-/-}$ BM, the pharmacological inhibition of TLR4 signaling after TAK-242 administration at 48 h did not significantly affect ECM accumulation and intrahepatic expression of MMPs (Figures 3B and 3D). In *Tlr4*$^{-/-}$ mice transplanted with WT BM, the pharmacological inhibition of TLR4 signaling with TAK-242 demonstrated significantly higher ECM accumulation and downregulation of hepatic MMP12 (Figures 3C and 3E). Ly6C expression and frequency in CD11b^{+} macrophages did not change in both chimeras (Figures S4B and S4C).

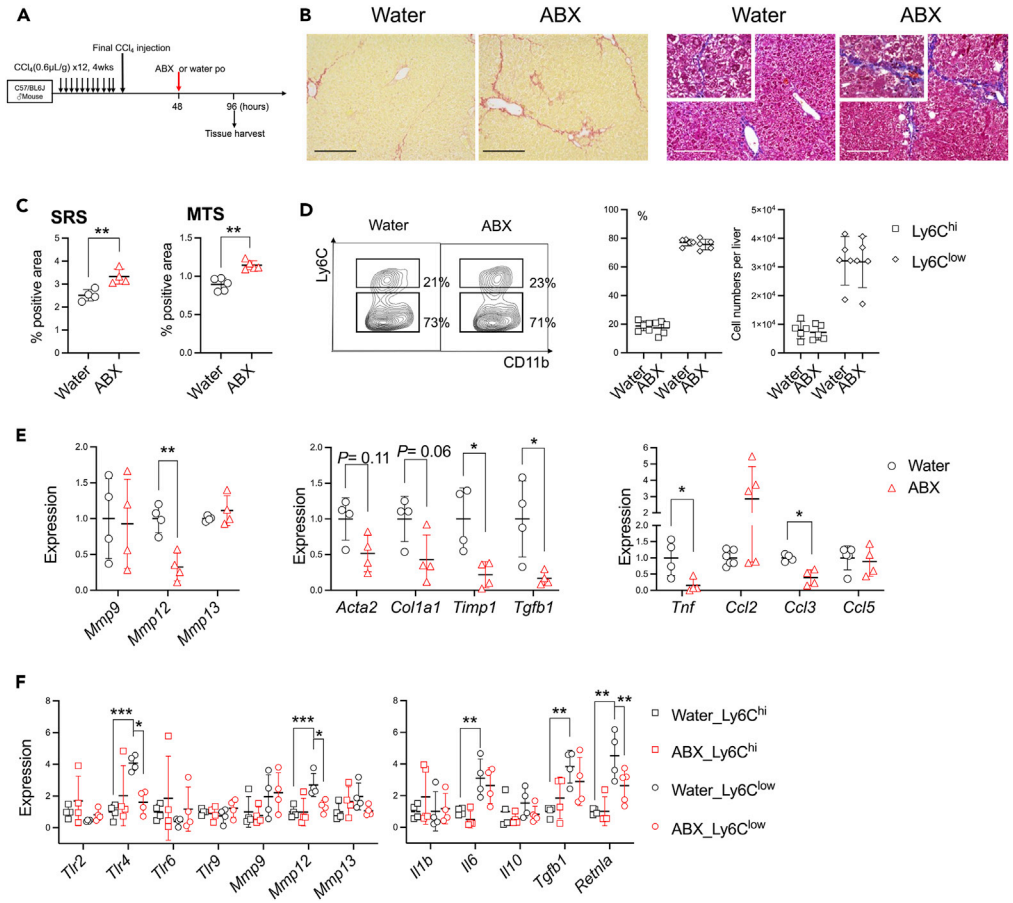

Figure 4. Gut Sterilization during liver fibrosis resolution

(A) Schematic representation.

(B) Representative hepatic photomicrographs of sirius red (left), Masson trichrome (right)—stained sections, accompanied with a 4-time magnification demonstrating portal to portal areas. A scale bar represents 500μm.

(C) Quantification of stained areas observed with sirius red staining (SRS) and Masson trichrome staining (MTS) by morphometric pixel analyses (n = 4–5).

(D) Representative Ly6C staining of $CD45^+$ $CD11b^+$ liver mononuclear cells (left), intrahepatic percentages (middle) and cell numbers (per liver; right) of $Ly6C^{hi}$ or $Ly6C^{low}$ among $CD11b^+$ macrophages (n = 5).

(E) Quantitative RT-PCR analysis of featured genes of the livers relative to water group (open circles, n = 4–5).

(F) Quantitative RT-PCR analysis of featured genes of flow cytometry-sorted intrahepatic $Ly6C^{hi}$ or $Ly6C^{low}$ $CD11b^+$ macrophages relative to water-treated $Ly6C^{hi}$ $CD11b^+$ macrophages (open squares, n = 4–5). Data show the mean ± SD. *p < 0.05, **p < 0.01, ***p < 0.001, unless otherwise specified. See also Figure S5.

Therefore, TLR4 signaling in BM-derived cells, rather than in non-BM-derived parenchymal cells, is indispensable for liver fibrosis resolution.

Significant delay of liver fibrosis resolution by gut sterilization is dependent on TLR4

To clarify the roles of gut commensal microbiota during liver fibrosis resolution, gut sterilization was performed as shown in Figure 4A. Significant higher levels of hepatic ECM accumulation were observed at 96 h in ABX (gut sterilization) group (Figures 4B and 4C), indicating delay of liver fibrosis resolution with gut sterilization. Gut sterilization didn't influence the frequency of $Ly6C^{low}$ macrophages (Figure 4D). Gut sterilization downregulated MMP12, similar to TAK-242 (Figure 1G), while expression of HSC activation markers decreased (Figure 4E). The decreased expression of hepatic *Tnf* and *Ccl3*, but not *Ccl2* or *Ccl5*, coincided with the delay in resolution (Figure 4E, right). After flow cytometry sorting exclusive of $T(CD3e^+)$, $B(CD19^+)$ and $NK(NK1.1^+)$ cells, the restorative $Ly6C^{low}$ $CD11b^+$ macrophages expressed significantly lower levels of *Tlr4* and *Mmp12* post-gut sterilization (Figure 4F). The existence of gut microbiota promotes liver fibrosis

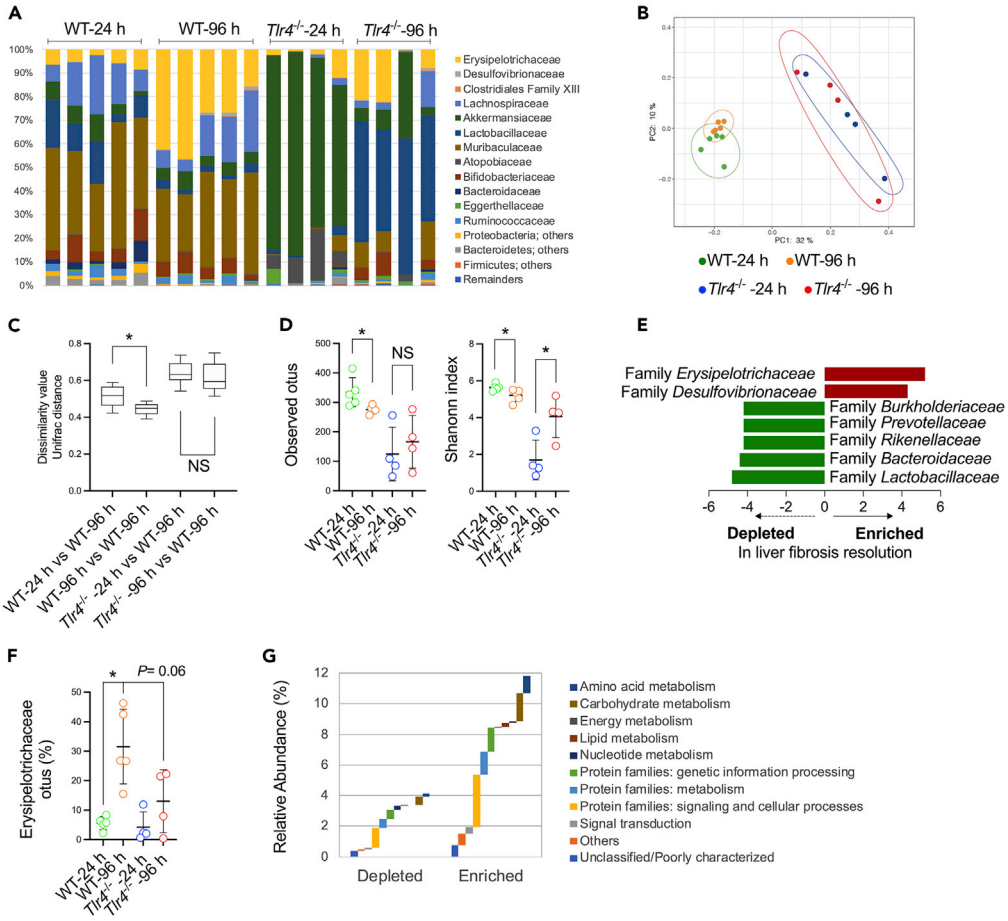

Figure 5. Metagenomic analysis during liver fibrosis resolution

(A) High-throughput sequencing of 16S rRNA during fecal bacterial DNA analysis at specific timepoints illustrated in Figure S1A.

(B) Principal coordinate analysis (PCoA) based on the unweighted UniFrac analysis of the bacterial community structures.

(C) The quantification of UniFrac distance in panel A, presented as dissimilarity values.

(D) The diversity of observed operational taxonomic units (OTUs) (left); α-diversity presented as Shannon indices (right).

(E) Linear discrimination analysis effect size (LEfSe) at the Family level showing significantly different gut microbiota taxonomies (linear discriminant analysis [LDA] score >3.6).

(F) The observed OTUs of Family Erysipelotrichaceae.

(G) Accumulated percentage of relative abundance of functional categories of KEGG Orthology Level 1 pathways significantly enriched or depleted in WT-96 h mice compared to those in WT-24 h mice, assessed by PICRUSt with LEfSE ($p < 0.05$; LDA >2). Data show the mean ± SD. *$p < 0.05$, unless otherwise specified. See also Table S1 and Figure S5.

resolution by enabling MMP12 and TLR4 upregulation in Ly6C^{low} CD11b^{+} restorative macrophages; this process is inhibited by gut sterilization. Contrarily, in *Tlr4*$^{-/-}$ mice (Figure S4D), gut sterilization did not significantly delay the resolution (Figure S4E) nor influenced the regulation of fibrosis-related markers and MMPs in *Tlr4*$^{-/-}$-administered mice (Figure S4G). Hence, TLR4 signaling is essential for the gut microbiota to promote liver fibrosis resolution.

Compositional and functional changes in the gut microbiota during liver fibrosis resolution

In metagenomic analyses comparing stools collected at peak of injury (24 h after last CCl_4 injection) and after resolution (96 h after last CCl_4 injection) in WT and *Tlr4*$^{-/-}$ mice, relative abundance at the family level (Figure 5A) and results of principal coordinate analysis (PCoA) of unweighted UniFrac (Figure 5B) demonstrated clustering of the gut microbiota in each group. Dissimilarity values calculated by the quantification of the UniFrac distances demonstrated a significant difference between 24 h and 96 h groups of WT mice,

but not between those of *Tlr4*$^{-/-}$ mice (Figure 5C). A post hoc combinational analysis of fecal materials from uninjured WT mice fed with normal diet demonstrated that these changes during resolution were disease-specific (Figure S5A). A minor but significant decrease in diversity, demonstrated by comparing bacterial operational taxonomic units (OTUs) and the Shannon index, was also noticed during resolution in WT mice (Figure 5D).

During the characterization of the microbiome by analyzing results of 16S rRNA high-throughput gene sequencing and LEfSe analysis, the proportion of family Erysipelotrichaceae (Phylum Firmicutes) increased significantly (LDA > 4.8), showing a dominating presence in the WT-96 h group compared to that in the WT-24 h group (Figures 5E, 5F, and S5B). A non-dominating proportion was also noticed in the family Desulfovibrionaceae (Figure S5C). Collectively, a significant increase of family Erysipelotrichaceae in abundance characterized the compositional change and decreased diversity in gut microbiota during CCl4-induced liver fibrosis resolution.

In PICRUSt analysis, the expression of 185 genes showed significant changes classified by KEGG Orthology functional categories Level 1 during liver fibrosis resolution, comparing between WT-24 h and WT-96 h groups (Table S1). Liver fibrosis resolution associated with significant shifts in the function of the gut microbiota with pathways related to energy metabolism and many various cellular signaling systems (Figure 5G). Whole-genome sequencing of isolated family Erysipelotrichaceae identified two specific strains (Figure S5D). Both strains possess bile salt hydrolase (BSH; KEGG enzyme 3.5.1.24), which is known for deconjugation of primary BAs (Figure S5E). Increased expression of *hdhA* (encoding 7-α hydroxysteroid dehydrogenase), the only upregulated gene related to BA metabolism during resolution observed in PICRUSt analysis (Table S1), also significantly correlated with the abundance of family Erysipelotrichaceae (Figure S5F). Hence, family *Erysipelotrichaceae*-related bile acid metabolism might be an influential functional change of gut microbiota during resolution.

Inhibition of TLR4 signaling and alteration of gut microbiome modified FXR-associated BA metabolism during liver fibrosis resolution

We next focused on how crosstalk between BA and gut microbiota impacts on post-injury withdrawal liver fibrosis resolution. Hepatic expression of various BA receptors was surveyed at the peak of fibrosis resolution (72 h) compared to that at the peak of liver injury (24 h). FXR (encoded by *Nr1h4*) was exclusively upregulated during resolution (Figure 6A). FXR and its related genes, as overviewed in Figure S6A, was focused. After the last CCl_4 injection, intrahepatic FXR was downregulated at the peak of liver injury (24 h) but upregulated during peak of resolution (72 h) (Figure 6B). This phenomenon was similar to what has been observed with CCl_4-induced acute liver injury.[17] Intrahepatic downstream effector genes of FXR were also examined. A similar trend of upregulation of small heterodimer partner (SHP, encoded by *Nr0b2*) was observed (Figure S6B). Intrahepatic expression levels of other downstream effector genes were also compared (Figure S6C). *Cyp7a1*, a master gene regulating bile acid synthesis, and *Foxm1b*, a gene regulating liver regeneration, were upregulated both with injury and during resolution, compared to uninjured controls. *Scl10a1* (encoding sodium-taurocholate co-transporting polypeptide; NTCP), a gene regulating bile acid reabsorption, also had a similar trend like *Nr1h4* (Figure 6B). In addition, increased intrahepatic protein levels of FXR and SHP during resolution were also confirmed by western blotting (Figure 6D).

Bile acids of fecal material and serum of portal vein were quantified by liquid chromatography-mass spectrometry at peak of liver injury (24 h) and during resolution (96 h) (Table S2). An increased fecal bile acid output, mainly unconjugated free bile acids without changes in hydrophobicity, was observed during resolution (Figures 6E and S6C). This finding might be partly explained by the dominance of BSH-expressing strains in the family Erysipelotrichaceae (Figures 5E, 5F, and S5E). Correlational analyses of ratios of various bile acid levels (96 h vs 24 h) were shown in Figure 6F. Noticeably, increased portal levels at 96 h of primary bile acids such as chenodeoxycholic acid (CDCA) and secondary bile acids such as 7-oxo- lithocholic acid (7-oxo-LCA), a metabolite of 7-α hydroxysteroid dehydrogenase, were significantly correlated with resolution. This finding is consistent with the increased expression of *hdhA* in the PICRUSt analysis (Table S1 and Figure S5F). A decreased level of portal tauro-β muricholic acid (TβMCA), a naturally occurring FXR antagonist,[29] was significantly correlated with resolution (Figure 6F).

Bile acid-related gene expression patterns were also analyzed in experiments with TAK-242. Significantly decreased levels of intrahepatic *Nr1h4* expression were observed with TLR4 inhibition by TAK-242 during

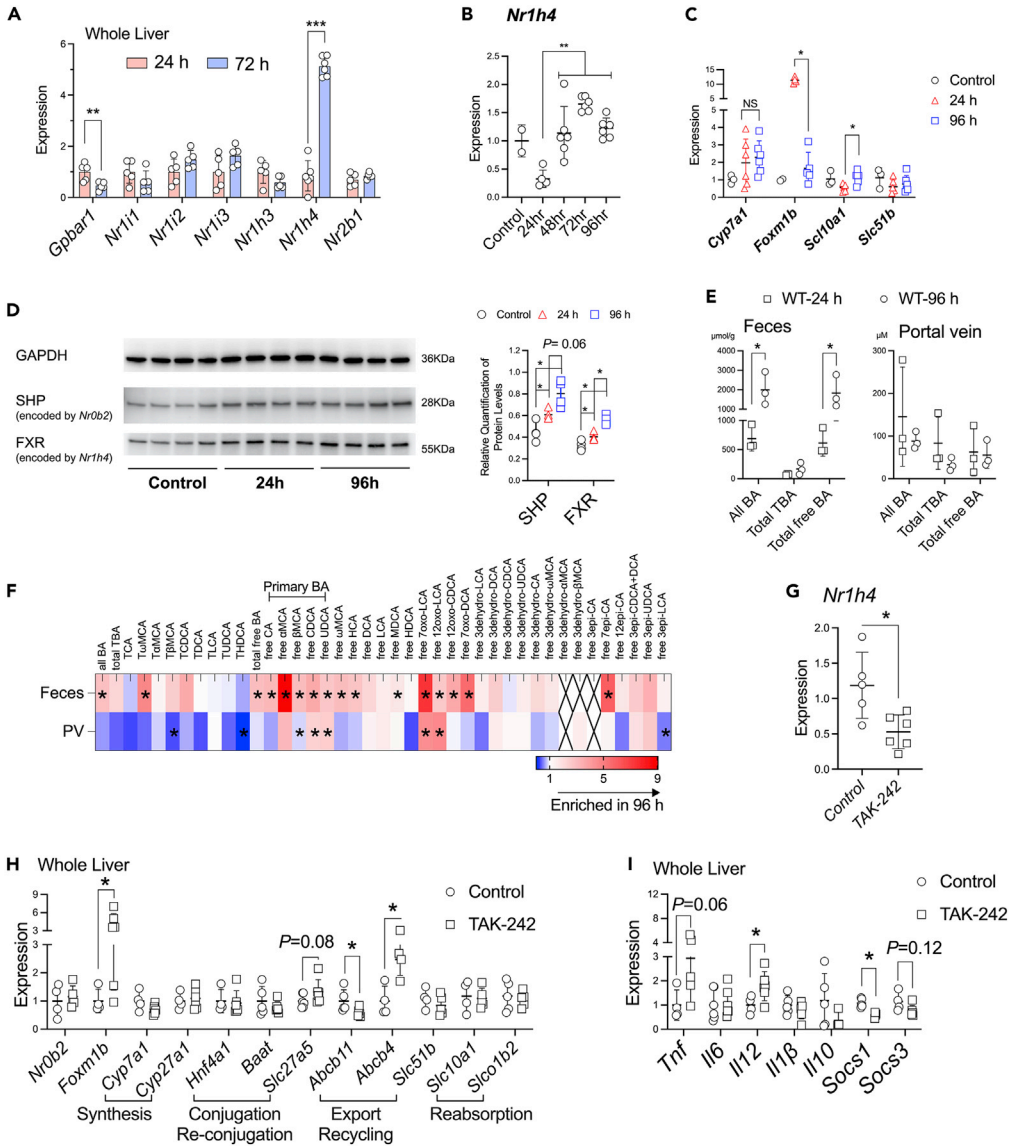

Figure 6. Bile acid metabolism during liver fibrosis resolution

(A) Quantitative RT-PCR analysis of featured genes of the livers relative to 24 h group (n = 4–5).

(B and C) Quantitative RT-PCR analysis of featured genes of the livers relative to control group (n = 4–5).

(D) Western blot analysis of featured proteins. Relative quantification of protein levels was compared. (n = 4).

(E) Bile acid composition of feces and portal vein during liver fibrosis resolution.

(F) Bile acid composition or ratios in feces and portal veins (PV) during liver fibrosis resolution demonstrating ratios of enrichment at 96 h after last CCl_4 injection. A cross mark designates any quantity below a detectable limit.

(G–I) Quantitative RT-PCR analysis of featured genes of the livers relative to control group in experiments represented in Figure 1A (n = 4–5). TBA, tauro-conjugated bile acids; TAK, TAK-242. Data show the mean ± SD. *p < 0.05, **p < 0.01, ***p < 0.001, unless otherwise specified. See also Figure S6.

resolution (Figure 6G). No significant change was observed with *Nr0b2, Cyp7a1*, or genes regarding bile acid reabsorption and conjugation. BA export marker *Abcb11* (encoding bile salt export protein; BSEP), a known FXR target gene, was downregulated, while another BA export maker *Abcb4* (encoding multidrug resistance protein 2; MDR2) was upregulated. BA re-conjugation marker *Slc27a5* was also upregulated (Figure 6H).

Regulation of FXR has been reported to be associated with cytokine activation.[17,30,31] The TLR4-inhibition-related downregulation of intrahepatic FXR (or delayed upregulation, as spontaneous upregulation was

observed in Figure 6B) during resolution might be associated with difference in recovery of inflammation. During resolution, upregulation of intrahepatic suppressor of cytokine signaling 1 (SOCS1), a negative regulator of TLR/NF-κB or STAT1 signaling, and SOCS3, another negative regulator of inflammatory pathways, was noticed (Figure S6D). Expression levels of *Tnf* and *Il12* were significantly higher under TLR4 inhibition during resolution, while those of *Socs1* and *Socs3* were lower (Figure 6I). These findings might be associated with a possible regulatory pathway for FXR in liver fibrosis resolution via TLR4 signaling.

Bile acids were also quantified in experiment of gut sterilization. Increased levels of both fecal and portal compositions of taurine-conjugated BAs and increased hydrophobicity (Figure S6C), possibly due to depletion of deconjugating gut microbiota, were noticed. Gut sterilization also dramatically altered the BA-FXR axis in both ileum and liver (Figures S6E and S6F). Gut sterilization also significantly depressed portal levels of CDCA and 7-oxo-LCA, and increased TβMCA (Figure S6G) which was contrary to what was observed during fibrosis resolution (Figure 6F).

ECM-degrading phenotype of bone marrow-derived macrophages is dependent on TLR4 and FXR

Prior phagocytosis is a key feature of restorative macrophages.[8] We used a post-phagocytosis model with BM-derived macrophages (BMDMs) to demonstrate the mechanism underlying the influence of TLR4 signaling in restorative macrophage development *in vitro* (Figure 7A). After ingestion of hepatocyte debris, M0 macrophages derived from primary BMDMs downregulated Ly6C (Figure 7B), and significantly upregulated MMP12 (Figure 7C). This upregulation was suppressed by TAK-242 while maintaining a robust expression of *Mmp9*, *Mmp12*, and *Mmp13* in response to LPS (Figure 7C). However, the *Mmp* expression was not restored by ingestion of debris by hepatocytes or LPS stimulation of BMDMs derived from *Tlr4*$^{-/-}$ mice (Figure 7D). Meanwhile, TLR4 was upregulated after ingestion of hepatocyte debris (Figure 7E). In comparison with M0 macrophages from primary BMDMs, a global upregulation of inflammatory cytokines, chemokine CCL3, chemokine receptors, SOCS1, and SOCS3 was observed in WT but not in *Tlr4*$^{-/-}$ BMDMs (Figure 7F).

Interestingly, expression levels of *Nr1h4* were elevated in M0 macrophages after phagocytosis; this elevation was partially diminished by pre-treatment of TAK-242 (Figure 7G). 7-oxo-LCA, a secondary bile acid that increased with resolution (Figure 6F), upregulated MMP12 and TLR4 in post-phagocytic WT BMDMs. CDCA showed a weak ability to upregulate them, while TβMCA, a naturally occurring FXR antagonist, downregulated them (Figure 7H). The expression of *Mmp12* and *Tlr4* were also compared in BMDMs before and after phagocytosis of hepatocyte debris (Figure 7I). The upregulation was more prominent in M0 macrophages after phagocytosis; it was partially diminished by pre-treatment of (Z)-guggulsterone (GS), an FXR antagonist (Figure 7I).

Transplant with fecal material harvested from WT-96 h group promoted liver fibrosis resolution in germ-free mice

To verify the fibrosis-resolving effect of gut microbiota *in vivo*, we investigated whether fecal material transplant (FMT) influenced liver fibrosis resolution with the CCl_4-induced liver fibrosis resolution model in germ-free (GF) mice. In experiments illustrated in Figure 8A, mice transplanted with fecal material obtained from the WT-96 h group demonstrated more prominent liver fibrosis resolution than those transplanted with fecal material from the WT-24 h group or those not subjected to FMT (Figures 8B and 8C). A tendency of the upregulation of hepatic MMP12, and HMBG1 was noticed in GF mice subjected to FMT during resolution (Figure 8D). Thus, the fibrosis-resolving ability of fecal material was verified. Expression of TLR4 was increased in intrahepatic CD11b^{+} myeloid cells harvested from mice transplanted with fecal material obtained from the WT-96 h group (Figure 8E), without significant changes in Ly6C expression (Figure S7A).

We also noticed a similar up-regulation of hepatic FXR and its downstream effector genes such as *Nr0b2* (encoding SHP) and those involved in BA metabolism during resolution; these tendencies were enforced post-FMT (Figure 8F). FMT significantly increased total fecal or portal BAs and/or total free BAs (Figures S7B and S7C), and in turn, up-regulated ileal FGF15 and down-regulated ileal ASBT (encoded by *Slc10a2*) (Figure 8F). Secondary to total free BA ratios increased in the portal veins of mice subjected to FMT, especially in those with WT-96h, while hydrophobicity of bile acids decreased with FMT (Figure S7D). Fecal or portal taurine-conjugated BAs, such as TβMCA, were significantly correlated with sirius red positive area (shown in %, Figures 8G and S7E) that implicated delay of fibrosis resolution.

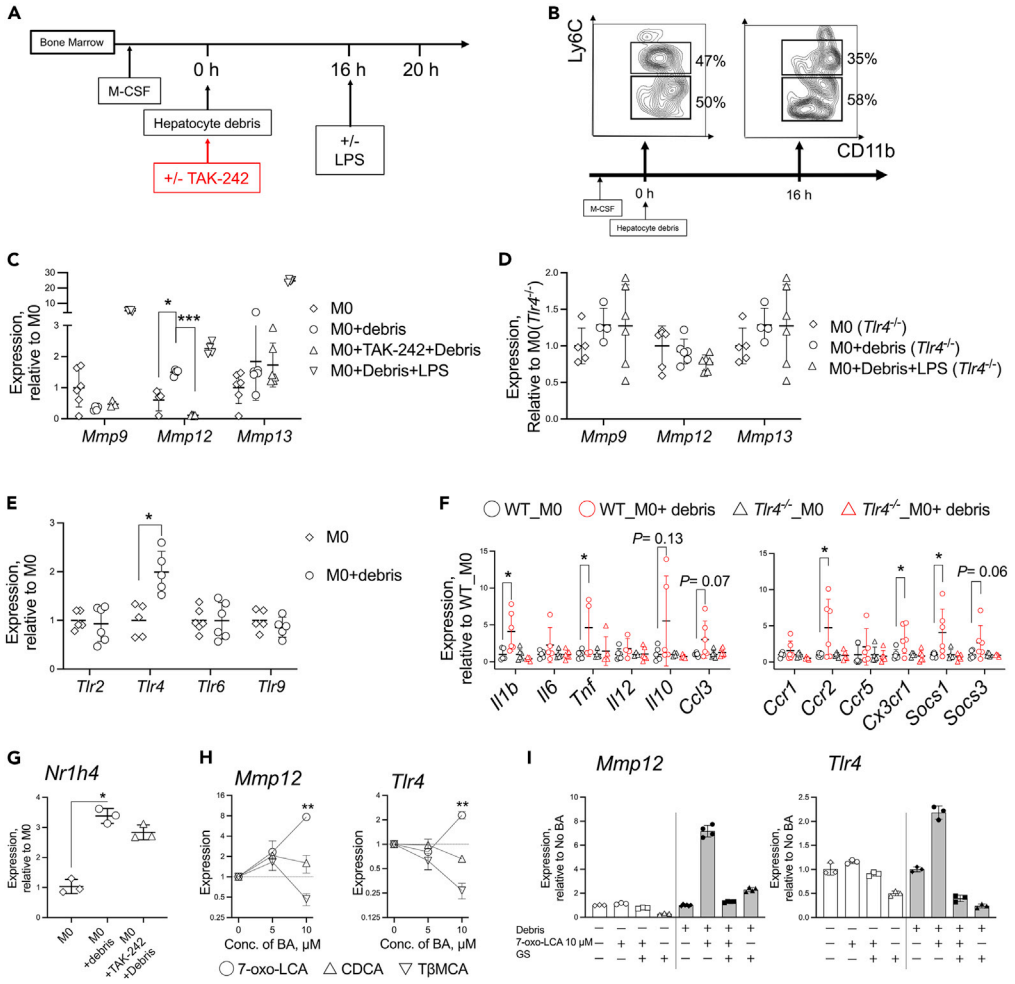

Figure 7. *In vitro* experiments utilizing post-phagocytic BMDMs

(A) Schematic representation of WT or *Tlr4*$^{-/-}$ bone marrow-derived macrophages (BMDMs) subjected to M0 induction (M-CSF), those treated with hepatocyte debris for phagocytosis or TAK-242, or those stimulated with lipopolysaccharide (LPS) *in vitro*.

(B) Representatives of CD11b and Ly6C staining by flow cytometry at indicated timepoints.

(C–I) Arbitrary ratios of the mRNA expression of MMPs, TLRs, or inflammatory markers were calculated relative to 18S rRNA in the treated BMDMs as specified (n = 5–6). In panels H and I, indicated bile acids were added 1 h after the hepatocyte debris. In panel I, relative expression was compared to M0 (white bars) or post-phagocytic BMDMs (gray bars) without pre-treatment of BAs, respectively. Data show the mean ± SD. *p < 0.05, **p < 0.01, ***p < 0.001, unless otherwise specified.

Elevation of serum HMGB1 and sCD14 associated with a liver fibrosis-resolving phenotype in CHC patients successfully treated with DAAs

Translational significance of our observations was also investigated. To figure out whether serological biomarkers related to TLR4 signaling associate with ECM remodeling early after HCV eradication, we focus on the serological dynamics of an intrinsic TLR4 ligand, HMGB1,[32] and soluble CD14 (sCD14), a co-receptor of TLR4,[33] in 23 CHC patients who successfully achieved HCV eradication with by interferon-free direct-acting agents (DAAs). Background characteristics were shown in Table S3. According to the dynamics of serum type IV collagen 7S fragment (4COL7S) and ELF, patients were classified into "early resolving (ER)", "delayed resolving (DR)" and "non-resolving (NR)" groups (Figures 9A and S8A and S8B). It is noteworthy that the phenotypes persisted longer than 1 year after end of treatment (EOT; Figure S8B), and correlated well with the MMP2/tissue inhibitor of metalloproteinases 1 (TIMP1) ratio, implicating a matrix-degrading phenotypes[34] with this classification (Figure S8C).

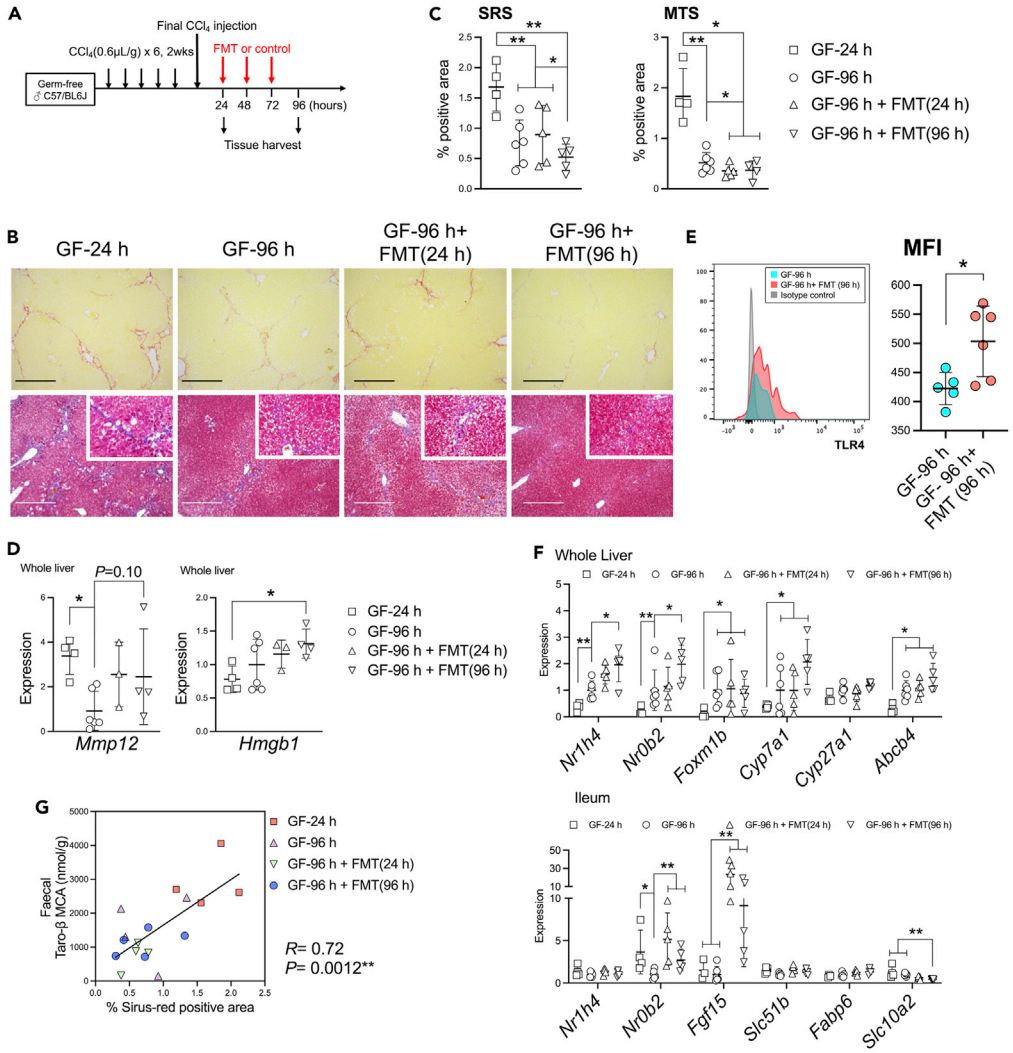

Figure 8. Transplantation with fecal material derived from WT 96 h promotes liver fibrosis resolution in germ-free mice

(A) Schematic representation of fecal material transplant (FMT) in germ-free (GF) mice.

(B) Representative hepatic photomicrographs of sirius red (left), Masson trichrome (right)—stained sections, accompanied with a 4-time magnification demonstrating portal to portal areas. A scale bar represents 500 μm.

(C) Quantification of stained areas observed with sirius red staining (SRS) and Masson trichrome staining (MTS) by morphometric pixel analyses (n = 4–5).

(D and F) Quantitative RT-PCR analysis of featured genes of the livers or ileum relative to GF-96 h group (n = 4–5).

(E) A representative of histogram of TLR4 expression in intrahepatic Ly6C^{low} CD11b^{+} macrophages at 96 h with or without FMT by flow cytometry. Mean fluorescence intensity (MFI) of TLR4 is shown. (n = 5).

(G) Correlation of percent-positive sirius red staining area to the levels of fecal tauro-β-MCA. Data show the mean ± SD. *p < 0.05, **p < 0.01, unless otherwise specified. See also Figure S7.

After the administration of DAAs, levels of serum ALT significantly decreased, and maintained as low levels through 12 weeks after EOT, implicative of a significant decrease in necro-inflammatory activity due to suppression of HCV replication (Figure 9B). In contrast to this trend, however, serum levels of HMGB1 and sCD14 remained elevated (Figures 9C and 9D). Normalized ALT and increased MMP2/TIMP1 ratio in the ER group implicated that the significant decrease of 4COL7S in not merely a result of decreased necro-inflammatory activity. At EOT, a timepoint where post-injury withdrawal resolution stands, higher levels of HMGB1 and sCD14 in the peripheral blood were observed in patients of ER group (Figures 9E and 9F), suggestive of a possible promotive role for liver fibrosis resolution of TLR4 signaling in theearly phase after suppression of HCV replication. Levels of HMGB1 and sCD14 were not associated with

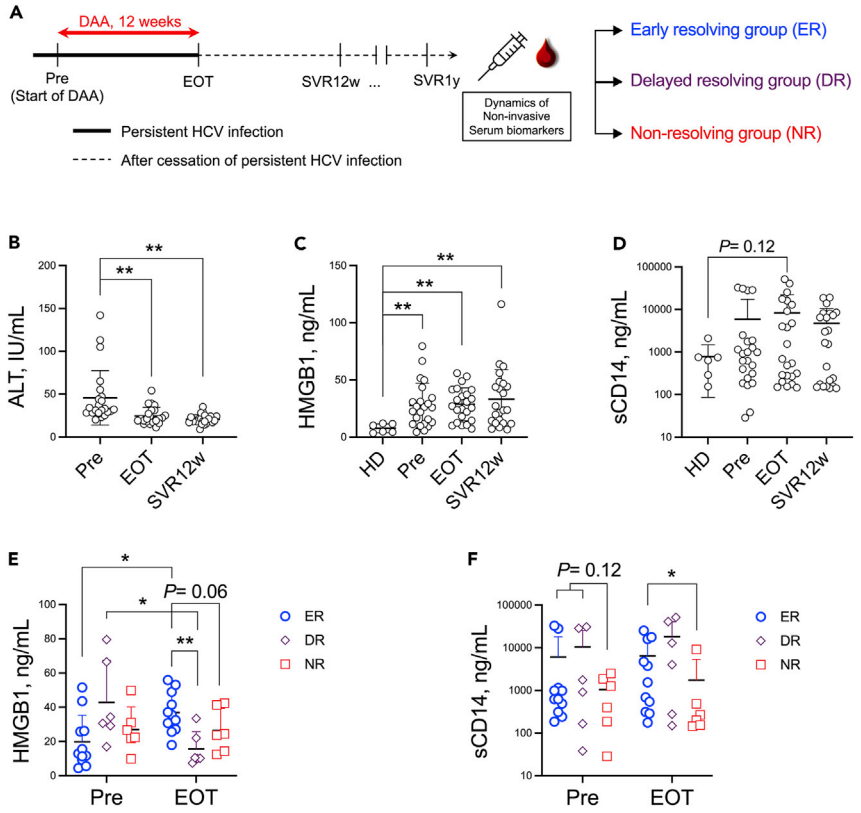

Figure 9. Higher levels of HMGB1 and sCD14 associated with a liver fibrosis-resolving phenotype in CHC patients treated with DAAs

(A) Schematic representation.

(B) Serum ALT levels just before start of treatment (Pre), at the end of treatment (EOT), and 12 weeks after the end of treatment achieving sustained virological response (SVR12w).

(C and D) Serum levels of HMGB1 (panel C) and soluble CD14 (sCD14; panel D) at the three timepoints indicated in panel B. HD, healthy donors.

(E and F) Serum levels of HMGB1 (panel E) and sCD14 (panel F) at Pre and EOT are compared by fibrosis-resolving phenotypes as defined in the Methods and Figure S8. Data show the mean ± SD. *p < 0.05, **p < 0.01, unless otherwise specified. See also Figure S8.

ALT levels at each timepoint (Figures S8D and S8E), suggesting that they were not markers for necro-inflammatory activity during post-injury withdrawal in the liver.

DISCUSSION

The results were summarized in Figure S9. Fitting into the concept of "holobiont,[35]" we demonstrated that in the early phase after persistent liver injury withdrawal, liver fibrosis resolution is associated with not only functional changes in myeloid TLR4 on the host side, but also shifts in various metabolic and signal transduction pathways in gut microbiome (Figure 5G and Table S1). Hepatic/ileal FXR signaling via the metabolism of BAs, the common products of the host and microbiome, is important for connecting both ends.

We demonstrated a beneficial role of TLR4 signaling and identified a link with a specific family of the gut microbiota (Family Erysipelotrichaceae) and CCl_4-induced liver fibrosis resolution in mice (Figures 5E and 5F). Mazagova and Wang et al. reported that germ-free mice demonstrated more severe CCl_4-induced liver fibrosis than conventionally raised mice. This phenomenon exacerbates as *Myd88/Trif*, the adaptor molecule of many toll-like receptors including TLR4, is genetically ablated.[15] It seemed to be conflicting to a pro-fibrogenetic role of LPS and TLR4 via TGF-β signaling in HSCs.[13] Our findings may suggest that a beneficial role of TLR4 exists during specifically the fibrosis resolution phase, at least early, especially

in myeloid cells. It is also note-worthy that with a NASH-diet murine model,[27] similar *Tlr4*-expressing features may also be observed in intrahepatic wound healing macrophages (Figures S3E and S3F). Because Erysipelotrichaceae members are significantly enriched in NAFLD patients with a lower degree of liver fibrosis,[36] further investigations examining its pro-fibrolytic applications as probiotics for patients with progressive liver diseases are warranted.

The plasticity and heterogeneity of macrophages have been examined during chronic inflammation.[37] Macrophages are a "double-edged sword" that are needed for both the physiological wounding process, fibrogenesis and fibrolysis ("the yin and yang"), maintaining homeostasis.[38,39] Questions remain in when, where, and how these phenotypical changes are regulated or controlled. We demonstrated how functional TLR4 signaling in macrophages is needed for this process. In scRNA-seq analysis, the distinct cluster of *Tlr4*-expressing CD11b^{+} Ly6C^{low} myeloid cells (MP (3) in Figure 2), presented similar scar-resolving phenotypes reported previously.[8,23] The existence of a cluster of Arg-1/CD14/TLR4 co-expressing macrophages during fibrosis resolution is also note-worthy (Figures 2G and 2H).

A functional inflammatory cascade provides such a "switch" for restorative macrophages to exert fibrolytic ability during liver fibrosis resolution.[8,40–42] We demonstrated possible mechanisms for regulation of this inflammatory cascade in restorative macrophages. Increased expression of *Mif*,[43] *Cstb*,[44] *AA467197* (also known as *Mir-147*[20]), or *Trem2*,[45] in the *Tlr4*-expressing intrahepatic myeloid cells during fibrosis resolution (Figures 3D and 3E), may exert immunoregulatory or anti-inflammatory function downstream of TLR4 signaling. In addition, CCL3, possibly upregulated downstream of functional TLR4 signaling in restorative macrophages, (Figures 1J, 4E, and 7F), may also exert a chemotaxic effect on natural killer (NK) and T cells,[46] a possible explanation for the accumulation of NK and T cells during liver fibrosis resolution (Figure S2E). It is congruent to the results of a previous report that cytotherapy with LPS/IFN-γ-stimulated M1 BMDMs recruits HSC apoptosis-inducing NK cells via CCL3.[10]

Another fine-tuning mechanism of TLR4 signaling during liver fibrolysis may be associated with the FXR. FXR signaling has been focused on its anti-inflammatory function,[30] however, how FXR influence the function of restorative macrophages is not elucidated. Our findings demonstrating (i) intrahepatic FXR down-regulation, or delayed recovery with pharmacological TLR4 inhibition during resolution *in vivo* (Figure 6G), (ii) FXR upregulation in post-phagocytic BMDM *in vrito* (Figure 7G), and (iii) MMP12 and TLR4 upregulation with FXR-agonizing bile acids in post-phagocytic BMDM *in vrito* (Figures 7H and 7I), may provide some clues. Our findings regarding the regulation of SOCS1 and SOCS3 (Figures 6I, S6D, and 7F) may provide some hints to connect TLR4 and FXR. FXR may upregulate SCOS3 to reduce hepatic inflammation.[47] SOCS1 suppresses IFN-γ/STAT1, which reciprocally regulates FXR in macrophages.[31] SOCS1 also suppresses TLR/NF-κB, which can be regulated via "transrepression" by various nuclear receptors, such as FXR.[48] Because many inflammatory cascades upregulate MMPs,[49] further investigations are needed to clarify how TLR-FXR interaction help maintaining restorative functions in post-phagocytotic macrophages, and how ECM-degrading MMPs are upregulated in these cells. Nonetheless, although we showed a prominent intrahepatic upregulation of FXR during resolution, the increase of bile acids such as LCA and DCA, two known TGR5 ligands, was also noticed (Figure 6F). We also noticed that regulation of many FXR-related genes cannot be simply explained by the regulation of intrahepatic FXR. It is still possible that other bile acid-related regulatory pathways other than FXR might be involved during resolution.

What are the ligands for TLR4 during liver fibrosis resolution? Although the gut sterilization demonstrated that post-injury withdrawal of liver fibrosis resolution could be modified by the existence of gut microbiota, a globally diminishing hepatic inflammation (Figure S1C) with waning of HSC activation (Figure S1D) during post-injury withdrawal resolution was observed. Therefore, LPS is unlikely to be the primary choice. Out observations showed upregulation of hepatic HMGB1, an intrinsic TLR4 ligand,[50] during post-injury withdrawal spontaneous resolution (Figure S1F) and after fecal material transplant to GF mice during resolution (Figure 8D). Sustained elevation of serum levels of HMGB1 after HCV treatment (Figure 9C), and the association of higher serum levels of HMGB1 and a fibrosis-resolving phenotype in CHC patients after HCV eradication (Figure 9E) also implicated a possible role of HMGB1. This current research is not sufficient to answer why regulation or expression of HMGB1 are maintained during liver fibrosis resolution in an SPF condition (Figure S1F), in germ-free mice (Figure 8D; comparing GF-24 h and GF-96 h), or in CHC patients after HCV eradication (Figures 9C and 9E); further investigations are needed.

To conclude, TLR4 signaling plays an essential role in murine liver fibrosis resolution after the withdrawal of liver injury. While the principal phenotype has been demonstrated with post withdrawal murine models, however, whether mechanistic features in humans could be mimicked needs to be further verified. Subsequent investigations may help develop more precise and novel pro-fibrolytic TLR4/FXR signaling-mediated cell therapy or possible probiotic/post-biotic applications in the future.

Limitations of the study

Although we utilized two murine models for in post-injury withdrawal fibrosis resolution in this study and demonstrated the existence of a cluster of restorative macrophages with similar transcriptional phenotypes in a murine NASH model with database analyses, a functional pro-fibrolytic role of TLR4 signaling in progressive liver diseases still needs to be verified. Due to the limitation of model, the roles of KC during resolution are also insufficiently explored. In the human study, a targeted quantification of two serum proteins associated with TLR4 only provided indirect clues. Additionally, the sample number of investigated CHC patients is small, and the lack of histological analyses may limit its translational significance. However, it is worth noticing that the best way for evaluation of degrees of liver fibrosis in CHC patients after HCV eradication is still indeterminate.[51] Further validations of our exploratory findings await.

STAR★METHODS

Detailed methods are provided in the online version of this paper and include the following:

- KEY RESOURCES TABLE
- RESOURCE AVAILABILITY
  - Lead contact
  - Materials availability
  - Data and code availability
- EXPERIMENTAL MODEL AND SUBJECT DETAILS
  - Patients
  - *In vivo* animal studies
  - Primary cultures
- METHOD DETAILS
  - Quantification of serum proteins
  - CCl_4 -induced liver fibrosis resolution model
  - MCD diet-induced liver fibrosis resolution model
  - TLR4 signaling inhibition
  - Assessment of liver injury and fibrosis
  - Hepatocyte debris preparation
  - Isolation of liver NPCs
  - Flow cytometry and FACS sorting
  - *In vivo* MMP activity assay
  - RNA extraction and RT-qPCR
  - Single-cell RNA-seq analysis
  - Gut sterilization
  - 16S rRNA metagenomic analysis
  - Metagenomic predictive functional profiling
  - Isolation of *Erysipelotrichaceae* bacterium
  - Whole genome analysis
  - Fecal material transplant
  - Bone marrow transplantation
  - Western blot analysis
  - Bile acid quantification
- QUANTIFICATION AND STATISTICAL ANALYSIS
  - Statistical analysis

SUPPLEMENTAL INFORMATION

Supplemental information can be found online at https://doi.org/10.1016/j.isci.2023.106220.

ACKNOWLEDGMENTS

This study was supported by grants-in-aid from Japan Society for the Promotion of Science (JSPS) KAKENHI (Grant Numbers 16K09373, 19K17502, and 22K08087 to P. Chu; 20H03666 to Y. Mikami and 20H00536 to T. Kanai); JSPS Grant-in-Aid for Transformative Research Areas(B): 21H05123 to YM; Advanced Research and Development Programs for Medical Innovation (AMED-CREST; 16gm1010003h0001 to T. Kanai, and 20gm1210001h0002 to YM, Practical Research Project for Rare/Intractable Diseases; 21ek0109556h0001 to Y. Mikami); grant-in-aid from the Miyakawa Memorial Research Foundation (2016-2017); and Keio University Medical Fund. None of them have any roles in study design, collection, analysis, and interpretation of data, and writing assistance. We are also thankful to Drs. Ryosuke Kasuga and Takaya Tabuchi for experimental assistance for revision of this study.

AUTHOR CONTRIBUTIONS

Conceptualization: YT, PC, NN, TK; Data curation: YT, PC, YH, YM, KM, RM, SF, TS, RI, MI, AH; Formal analysis: YT, PC, NN, YM, KM, RM, TT, NT, SF, TS, YK, RI, MI, AH; Funding acquisition: PC, YM, TK; Investigation: YT, PC, YH, YM, RM, TT, NT, SF, TS, YK, RI, MI, AH, TK; Methodology: YT, PC, NN, YH, YM, KM, TT, SF, YK, AH; Project administration: PC, NN, TK; Resources: PC, NN, YM, KM, TT, NT, AH, TK; Software: YT, PC, YM, KM, AH; Supervision: NN, TK; Validation: YT, PC, YH, YM, KM, RM, TT, NT, SF, TS, YK, RI, MI; Visualization: YT, PC, YM, KM; Writing- original draft: YT, PC; Writing-review & editing: PC, NN, YM, AH, TK; Final approval: all of the authors; Agreement to be accountable for all aspects of the work: all of the authors.

DECLARATION OF INTERESTS

The authors declare no competing interests.

INCLUSION AND DIVERSITY

We support inclusive, diverse, and equitable conduct of research.

Received: December 9, 2021
Revised: August 25, 2022
Accepted: February 13, 2023
Published: February 16, 2023

REFERENCES

1. Pellicoro, A., Ramachandran, P., Iredale, J.P., and Fallowfield, J.A. (2014). Liver fibrosis and repair: immune regulation of wound healing in a solid organ. Nat. Rev. Immunol. *14*, 181–194. https://doi.org/10.1038/nri3623.

2. D'Ambrosio, R., Aghemo, A., Rumi, M.G., Ronchi, G., Donato, M.F., Paradis, V., Colombo, M., and Bedossa, P. (2012). A morphometric and immunohistochemical study to assess the benefit of a sustained virological response in hepatitis C virus patients with cirrhosis. Hepatology *56*, 532–543. https://doi.org/10.1002/hep.25606.

3. Marcellin, P., Gane, E., Buti, M., Afdhal, N., Sievert, W., Jacobson, I.M., Washington, M.K., Germanidis, G., Flaherty, J.F., Aguilar Schall, R., et al. (2013). Regression of cirrhosis during treatment with tenofovir disoproxil fumarate for chronic hepatitis B: a 5-year open-label follow-up study. Lancet *381*, 468–475. https://doi.org/10.1016/S0140-6736(12)61425-1.

4. Vilar-Gomez, E., Martinez-Perez, Y., Calzadilla-Bertot, L., Torres-Gonzalez, A., Gra-Oramas, B., Gonzalez-Fabian, L., Friedman, S.L., Diago, M., and Romero-Gomez, M. (2015). Weight loss through lifestyle modification significantly reduces features of nonalcoholic steatohepatitis. Gastroenterology *149*, 367–378.e5. https://doi.org/10.1053/j.gastro.2015.04.005.

5. Lee, Y.A., Wallace, M.C., and Friedman, S.L. (2015). Pathobiology of liver fibrosis: a translational success story. Gut *64*, 830–841. https://doi.org/10.1136/gutjnl-2014-306842.

6. Lee, Y.A., and Friedman, S.L. (2014). Reversal, maintenance or progression: what happens to the liver after a virologic cure of hepatitis C? Antiviral Res. *107*, 23–30. https://doi.org/10.1016/j.antiviral.2014.03.012.

7. Seki, E., and Schwabe, R.F. (2015). Hepatic inflammation and fibrosis: functional links and key pathways. Hepatology *61*, 1066–1079. https://doi.org/10.1002/hep.27332.

8. Ramachandran, P., Pellicoro, A., Vernon, M.A., Boulter, L., Aucott, R.L., Ali, A., Hartland, S.N., Snowdon, V.K., Cappon, A., Gordon-Walker, T.T., et al. (2012). Differential Ly-6C expression identifies the recruited macrophage phenotype, which orchestrates the regression of murine liver fibrosis. Proc. Natl. Acad. Sci. USA *109*, E3186–E3195. https://doi.org/10.1073/pnas.1119964109.

9. Sakaida, I., Terai, S., Yamamoto, N., Aoyama, K., Ishikawa, T., Nishina, H., and Okita, K. (2004). Transplantation of bone marrow cells reduces CCl4-induced liver fibrosis in mice. Hepatology *40*, 1304–1311. https://doi.org/10.1002/hep.20452.

10. Ma, P.F., Gao, C.C., Yi, J., Zhao, J.L., Liang, S.Q., Zhao, Y., Ye, Y.C., Bai, J., Zheng, Q.J., Dou, K.F., et al. (2017). Cytotherapy with M1-polarized macrophages ameliorates liver fibrosis by modulating immune microenvironment in mice. J. Hepatol. *67*, 770–779. https://doi.org/10.1016/j.jhep.2017.05.022.

11. Crispe, I.N. (2009). The liver as a lymphoid organ. Annu. Rev. Immunol. *27*, 147–163. https://doi.org/10.1146/annurev.immunol.021908.132629.

12. Seki, E., and Brenner, D.A. (2008). Toll-like receptors and adaptor molecules in liver disease: update. Hepatology *48*, 322–335. https://doi.org/10.1002/hep.22306.

13. Seki, E., De Minicis, S., Osterreicher, C.H., Kluwe, J., Osawa, Y., Brenner, D.A., and Schwabe, R.F. (2007). TLR4 enhances TGF-beta signaling and hepatic fibrosis. Nat. Med.

13, 1324–1332. https://doi.org/10.1038/nm1663.

14. Kumar, S., Wang, J., Shanmukhappa, S.K., and Gandhi, C.R. (2017). Toll-like receptor 4-independent carbon tetrachloride-induced fibrosis and lipopolysaccharide-induced acute liver injury in mice: role of hepatic stellate cells. Am. J. Pathol. *187*, 1356–1367. https://doi.org/10.1016/j.ajpath.2017.01.021.

15. Mazagova, M., Wang, L., Anfora, A.T., Wissmueller, M., Lesley, S.A., Miyamoto, Y., Eckmann, L., Dhungana, S., Pathmasiri, W., Sumner, S., et al. (2015). Commensal microbiota is hepatoprotective and prevents liver fibrosis in mice. FASEB J. *29*, 1043–1055. https://doi.org/10.1096/fj.14-259515.

16. Schneider, K.M., Mohs, A., Kilic, K., Candels, L.S., Elfers, C., Bennek, E., Schneider, L.B., Heymann, F., Gassler, N., Penders, J., and Trautwein, C. (2019). Intestinal microbiota protects against MCD diet-induced steatohepatitis. Int. J. Mol. Sci. *20*, 308. https://doi.org/10.3390/ijms20020308.

17. Meng, Z., Wang, Y., Wang, L., Jin, W., Liu, N., Pan, H., Liu, L., Wagman, L., Forman, B.M., and Huang, W. (2010). FXR regulates liver repair after CCl4-induced toxic injury. Mol. Endocrinol. *24*, 886–897. https://doi.org/10.1210/me.2009-0286.

18. Kawamoto, T., Ii, M., Kitazaki, T., Iizawa, Y., and Kimura, H. (2008). TAK-242 selectively suppresses Toll-like receptor 4-signaling mediated by the intracellular domain. Eur. J. Pharmacol. *584*, 40–48. https://doi.org/10.1016/j.ejphar.2008.01.026.

19. Karamanos, N.K., Theocharis, A.D., Piperigkou, Z., Manou, D., Passi, A., Skandalis, S.S., Vynios, D.H., Orian-Rousseau, V., Ricard-Blum, S., Schmelzer, C.E.H., et al. (2021). A guide to the composition and functions of the extracellular matrix. FEBS J. *288*, 6850–6912. https://doi.org/10.1111/febs.15776.

20. Liu, G., Friggeri, A., Yang, Y., Park, Y.J., Tsuruta, Y., and Abraham, E. (2009). miR-147, a microRNA that is induced upon Toll-like receptor stimulation, regulates murine macrophage inflammatory responses. Proc. Natl. Acad. Sci. USA *106*, 15819–15824. https://doi.org/10.1073/pnas.0901216106.

21. Heinrichs, D., Knauel, M., Offermanns, C., Berres, M.L., Nellen, A., Leng, L., Schmitz, P., Bucala, R., Trautwein, C., Weber, C., et al. (2011). Macrophage migration inhibitory factor (MIF) exerts antifibrotic effects in experimental liver fibrosis via CD74. Proc. Natl. Acad. Sci. USA *108*, 17444–17449. https://doi.org/10.1073/pnas.1107023108.

22. Sobrevals, L., Rodriguez, C., Romero-Trevejo, J.L., Gondi, G., Monreal, I., Pañeda, A., Juanarena, N., Arcelus, S., Razquin, N., Guembe, L., et al. (2010). Insulin-like growth factor I gene transfer to cirrhotic liver induces fibrolysis and reduces fibrogenesis leading to cirrhosis reversion in rats. Hepatology *51*, 912–921. https://doi.org/10.1002/hep.23412.

23. Ramachandran, P., Dobie, R., Wilson-Kanamori, J.R., Dora, E.F., Henderson, B.E.P., Luu, N.T., Portman, J.R., Matchett, K.P., Brice, M., Marwick, J.A., et al. (2019). Resolving the fibrotic niche of human liver cirrhosis at single-cell level. Nature *575*, 512–518. https://doi.org/10.1038/s41586-019-1631-3.

24. Satpathy, A.T., Kc, W., Albring, J.C., Edelson, B.T., Kretzer, N.M., Bhattacharya, D., Murphy, T.L., and Murphy, K.M. (2012). Zbtb46 expression distinguishes classical dendritic cells and their committed progenitors from other immune lineages. J. Exp. Med. *209*, 1135–1152. https://doi.org/10.1084/jem.20120030.

25. Bennett, H., Troutman, T.D., Sakai, M., and Glass, C.K. (2020). Epigenetic regulation of kupffer cell function in health and disease. Front. Immunol. *11*, 609618. https://doi.org/10.3389/fimmu.2020.609618.

26. Brown, C.C., Gudjonson, H., Pritykin, Y., Deep, D., Lavallée, V.P., Mendoza, A., Fromme, R., Mazutis, L., Ariyan, C., Leslie, C., et al. (2019). Transcriptional basis of mouse and human dendritic cell heterogeneity. Cell *179*, 846–863.e24. https://doi.org/10.1016/j.cell.2019.09.035.

27. Seidman, J.S., Troutman, T.D., Sakai, M., Gola, A., Spann, N.J., Bennett, H., Bruni, C.M., Ouyang, Z., Li, R.Z., Sun, X., et al. (2020). Niche-specific reprogramming of epigenetic landscapes drives myeloid cell diversity in nonalcoholic steatohepatitis. Immunity *52*, 1057–1074.e7. https://doi.org/10.1016/j.immuni.2020.04.001.

28. Amiya, T., Nakamoto, N., Chu, P.S., Teratani, T., Nakajima, H., Fukuchi, Y., Taniki, N., Yamaguchi, A., Shiba, S., Miyake, R., et al. (2016). Bone marrow-derived macrophages distinct from tissue-resident macrophages play a pivotal role in Concanavalin A-induced murine liver injury via CCR9 axis. Sci. Rep. *6*, 35146. https://doi.org/10.1038/srep35146.

29. Sayin, S.I., Wahlström, A., Felin, J., Jäntti, S., Marschall, H.U., Bamberg, K., Angelin, B., Hyötyläinen, T., Orešič, M., and Bäckhed, F. (2013). Gut microbiota regulates bile acid metabolism by reducing the levels of tauro-beta-muricholic acid, a naturally occurring FXR antagonist. Cell Metab. *17*, 225–235. https://doi.org/10.1016/j.cmet.2013.01.003.

30. Bertolini, A., Fiorotto, R., and Strazzabosco, M. (2022). Bile acids and their receptors: modulators and therapeutic targets in liver inflammation. Semin. Immunopathol. *44*, 547–564. https://doi.org/10.1007/s00281-022-00935-7.

31. Renga, B., Migliorati, M., Mencarelli, A., and Fiorucci, S. (2009). Reciprocal regulation of the bile acid-activated receptor FXR and the interferon-gamma-STAT-1 pathway in macrophages. Biochim. Biophys. Acta *1792*, 564–573. https://doi.org/10.1016/j.bbadis.2009.04.004.

32. Mencin, A., Kluwe, J., and Schwabe, R.F. (2009). Toll-like receptors as targets in chronic liver diseases. Gut *58*, 704–720. https://doi.org/10.1136/gut.2008.156307.

33. Frey, E.A., Miller, D.S., Jahr, T.G., Sundan, A., Bazil, V., Espevik, T., Finlay, B.B., and Wright, S.D. (1992). Soluble CD14 participates in the response of cells to lipopolysaccharide. J. Exp. Med. *176*, 1665–1671. https://doi.org/10.1084/jem.176.6.1665.

34. Hemmann, S., Graf, J., Roderfeld, M., and Roeb, E. (2007). Expression of MMPs and TIMPs in liver fibrosis - a systematic review with special emphasis on anti-fibrotic strategies. J. Hepatol. *46*, 955–975. https://doi.org/10.1016/j.jhep.2007.02.003.

35. Lynch, S.V., and Pedersen, O. (2016). The human intestinal microbiome in health and disease. N. Engl. J. Med. *375*, 2369–2379. https://doi.org/10.1056/NEJMra1600266.

36. Boursier, J., Mueller, O., Barret, M., Machado, M., Fizanne, L., Araujo-Perez, F., Guy, C.D., Seed, P.C., Rawls, J.F., David, L.A., et al. (2016). The severity of nonalcoholic fatty liver disease is associated with gut dysbiosis and shift in the metabolic function of the gut microbiota. Hepatology *63*, 764–775. https://doi.org/10.1002/hep.28356.

37. Parisi, L., Gini, E., Baci, D., Tremolati, M., Fanuli, M., Bassani, B., Farronato, G., Bruno, A., and Mortara, L. (2018). Macrophage polarization in chronic inflammatory diseases: killers or builders? J. Immunol. Res. *2018*, 8917804. https://doi.org/10.1155/2018/8917804.

38. Friedman, S.L. (2005). Mac the knife? Macrophages- the double-edged sword of hepatic fibrosis. J. Clin. Invest. *115*, 29–32. https://doi.org/10.1172/JCI23928.

39. Sica, A., Invernizzi, P., and Mantovani, A. (2014). Macrophage plasticity and polarization in liver homeostasis and pathology. Hepatology *59*, 2034–2042. https://doi.org/10.1002/hep.26754.

40. Stock, M.K., Hammerich, L., do O, N.T., Berres, M.L., Alsamman, M., Heinrichs, D., Nellen, A., Trautwein, C., Tacke, F., Wasmuth, H.E., and Sahin, H. (2013). Met-CCL5 modifies monocyte subpopulations during liver fibrosis regression. Int. J. Clin. Exp. Pathol. *6*, 678–685.

41. Campana, L., Starkey Lewis, P.J., Pellicoro, A., Aucott, R.L., Man, J., O'Duibhir, E., Mok, S.E., Ferreira-Gonzalez, S., Livingstone, E., Greenhalgh, S.N., et al. (2018). The STAT3-IL-10-IL-6 pathway is a novel regulator of macrophage efferocytosis and phenotypic conversion in sterile liver injury. J. Immunol. *200*, 1169–1187. https://doi.org/10.4049/jimmunol.1701247.

42. Krenkel, O., Puengel, T., Govaere, O., Abdallah, A.T., Mossanen, J.C., Kohlhepp, M., Liepelt, A., Lefebvre, E., Luedde, T., Hellerbrand, C., et al. (2018). Therapeutic inhibition of inflammatory monocyte recruitment reduces steatohepatitis and liver fibrosis. Hepatology *67*, 1270–1283. https://doi.org/10.1002/hep.29544.

43. Roger, T., David, J., Glauser, M.P., and Calandra, T. (2001). MIF regulates innate immune responses through modulation of Toll-like receptor 4. Nature *414*, 920–924. https://doi.org/10.1038/414920a.

44. Maher, K., Završnik, J., Jerič-Kokelj, B., Vasiljeva, O., Turk, B., and Kopitar-Jerala, N. (2014). Decreased IL-10 expression in stefin

B-deficient macrophages is regulated by the MAP kinase and STAT-3 signaling pathways. FEBS Lett. *588*, 720–726. https://doi.org/10.1016/j.febslet.2014.01.015.

45. Turnbull, I.R., Gilfillan, S., Cella, M., Aoshi, T., Miller, M., Piccio, L., Hernandez, M., and Colonna, M. (2006). Cutting edge: TREM-2 attenuates macrophage activation. J. Immunol. *177*, 3520–3524. https://doi.org/10.4049/jimmunol.177.6.3520.

46. Marra, F., and Tacke, F. (2014). Roles for chemokines in liver disease. Gastroenterology *147*, 577–594.e1. https://doi.org/10.1053/j.gastro.2014.06.043.

47. Xu, Z., Huang, G., Gong, W., Zhou, P., Zhao, Y., Zhang, Y., Zeng, Y., Gao, M., Pan, Z., and He, F. (2012). FXR ligands protect against hepatocellular inflammation via SOCS3 induction. Cell. Signal. *24*, 1658–1664. https://doi.org/10.1016/j.cellsig.2012.04.015.

48. Hollman, D.A.A., Milona, A., van Erpecum, K.J., and van Mil, S.W.C. (2012). Anti-inflammatory and metabolic actions of FXR: insights into molecular mechanisms. Biochim. Biophys. Acta *1821*, 1443–1452. https://doi.org/10.1016/j.bbalip.2012.07.004.

49. Fanjul-Fernández, M., Folgueras, A.R., Cabrera, S., and López-Otín, C. (2010). Matrix metalloproteinases: evolution, gene regulation and functional analysis in mouse models. Biochim. Biophys. Acta *1803*, 3–19. https://doi.org/10.1016/j.bbamcr.2009.07.004.

50. Gaskell, H., Ge, X., and Nieto, N. (2018). High-mobility group box-1 and liver disease. Hepatol. Commun. *2*, 1005–1020. https://doi.org/10.1002/hep4.1223.

51. European Association for the Study of the Liver Electronic address easloffice@easlofficeeu; Clinical Practice Guideline Panel, Chair:; EASL Governing Board representative:; Panel members: (2021). EASL Clinical Practice Guidelines on non-invasive tests for evaluation of liver disease severity and prognosis - 2021 update. J. Hepatol. *75*, 659–689. https://doi.org/10.1016/j.jhep.2021.05.025.

52. Allen, I.C. (2013). Mouse Models of Innate Immunity : Methods and Protocols (Humana Press).

53. Cai, Y., Kumai, S., Ogawa, M., Benno, Y., and Nakase, T. (1999). Characterization and identification of Pediococcus species isolated from forage crops and their application for silage preparation. Appl. Environ. Microbiol. *65*, 2901–2906. https://doi.org/10.1128/AEM.65.7.2901-2906.1999.

54. Nakamoto, N., Sasaki, N., Aoki, R., Miyamoto, K., Suda, W., Teratani, T., Suzuki, T., Koda, Y., Chu, P.S., Taniki, N., et al. (2019). Gut pathobionts underlie intestinal barrier dysfunction and liver T helper 17 cell immune response in primary sclerosing cholangitis. Nat. Microbiol. *4*, 492–503. https://doi.org/10.1038/s41564-018-0333-1.

55. Seemann, T. (2014). Prokka: rapid prokaryotic genome annotation. Bioinformatics *30*, 2068–2069. https://doi.org/10.1093/bioinformatics/btu153.

56. Kanehisa, M., Sato, Y., and Morishima, K. (2016). BlastKOALA and GhostKOALA: KEGG tools for functional characterization of genome and metagenome sequences. J. Mol. Biol. *428*, 726–731. https://doi.org/10.1016/j.jmb.2015.11.006.

57. Matsunaga, N., Tsuchimori, N., Matsumoto, T., and Ii, M. (2011). TAK-242 (resatorvid), a small-molecule inhibitor of Toll-like receptor (TLR) 4 signaling, binds selectively to TLR4 and interferes with interactions between TLR4 and its adaptor molecules. Mol. Pharmacol. *79*, 34–41. https://doi.org/10.1124/mol.110.068064.

58. Teratani, T., Tomita, K., Suzuki, T., Furuhashi, H., Irie, R., Hida, S., Okada, Y., Kurihara, C., Ebinuma, H., Nakamoto, N., et al. (2017). Free cholesterol accumulation in liver sinusoidal endothelial cells exacerbates acetaminophen hepatotoxicity via TLR9 signaling. J. Hepatol. *67*, 780–790. https://doi.org/10.1016/j.jhep.2017.05.020.

59. Chu, P.S., Nakamoto, N., Ebinuma, H., Usui, S., Saeki, K., Matsumoto, A., Mikami, Y., Sugiyama, K., Tomita, K., Kanai, T., et al. (2013). C-C motif chemokine receptor 9 positive macrophages activate hepatic stellate cells and promote liver fibrosis in mice. Hepatology *58*, 337–350. https://doi.org/10.1002/hep.26351.

60. Mikami, Y., Philips, R.L., Sciumè, G., Petermann, F., Meylan, F., Nagashima, H., Yao, C., Davis, F.P., Brooks, S.R., Sun, H.W., et al. (2021). MicroRNA-221 and -222 modulate intestinal inflammatory Th17 cell response as negative feedback regulators downstream of interleukin-23. Immunity *54*, 514–525.e6. https://doi.org/10.1016/j.immuni.2021.02.015.

61. Macosko, E.Z., Basu, A., Satija, R., Nemesh, J., Shekhar, K., Goldman, M., Tirosh, I., Bialas, A.R., Kamitaki, N., Martersteck, E.M., et al. (2015). Highly parallel genome-wide expression profiling of individual cells using nanoliter droplets. Cell *161*, 1202–1214. https://doi.org/10.1016/j.cell.2015.05.002.

62. Satija, R., Farrell, J.A., Gennert, D., Schier, A.F., and Regev, A. (2015). Spatial reconstruction of single-cell gene expression data. Nat. Biotechnol. *33*, 495–502. https://doi.org/10.1038/nbt.3192.

63. Nakamoto, N., Amiya, T., Aoki, R., Taniki, N., Koda, Y., Miyamoto, K., Teratani, T., Suzuki, T., Chiba, S., Chu, P.S., et al. (2017). Commensal lactobacillus controls immune tolerance during acute liver injury in mice. Cell Rep. *21*, 1215–1226. https://doi.org/10.1016/j.celrep.2017.10.022.

64. Xu, L., Surathu, A., Raplee, I., Chockalingam, A., Stewart, S., Walker, L., Sacks, L., Patel, V., Li, Z., and Rouse, R. (2020). The effect of antibiotics on the gut microbiome: a metagenomics analysis of microbial shift and gut antibiotic resistance in antibiotic treated mice. BMC Genom. *21*, 263. https://doi.org/10.1186/s12864-020-6665-2.

65. Amiya, T., Nakamoto, N., Irie, J., Taniki, N., Chu, P.S., Koda, Y., Miyamoto, K., Yamaguchi, A., Shiba, S., Morikawa, R., et al. (2021). C-C motif chemokine receptor 9 regulates obesity-induced insulin resistance via inflammation of the small intestine in mice. Diabetologia *64*, 603–617. https://doi.org/10.1007/s00125-020-05349-4.

66. Douglas, G.M., Maffei, V.J., Zaneveld, J.R., Yurgel, S.N., Brown, J.R., Taylor, C.M., Huttenhower, C., and Langille, M.G.I. (2020). PICRUSt2 for prediction of metagenome functions. Nat. Biotechnol. *38*, 685–688. https://doi.org/10.1038/s41587-020-0548-6.

67. Honda, A., Miyazaki, T., Iwamoto, J., Hirayama, T., Morishita, Y., Monma, T., Ueda, H., Mizuno, S., Sugiyama, F., Takahashi, S., and Ikegami, T. (2020). Regulation of bile acid metabolism in mouse models with hydrophobic bile acid composition. J. Lipid Res. *61*, 54–69. https://doi.org/10.1194/jlr.RA119000395.

68. Murakami, M., Iwamoto, J., Honda, A., Tsuji, T., Tamamushi, M., Ueda, H., Monma, T., Konishi, N., Yara, S., Hirayama, T., et al. (2018). Detection of gut dysbiosis due to reduced Clostridium subcluster XIVa using the fecal or serum bile acid profile. Inflamm. Bowel Dis. *24*, 1035–1044. https://doi.org/10.1093/ibd/izy022.

69. Heuman, D.M., Hylemon, P.B., and Vlahcevic, Z.R. (1989). Regulation of bile acid synthesis. III. Correlation between biliary bile salt hydrophobicity index and the activities of enzymes regulating cholesterol and bile acid synthesis in the rat. J. Lipid Res. *30*, 1161–1171.

STAR★METHODS

KEY RESOURCES TABLE

REAGENT or RESOURCE	SOURCE	IDENTIFIER
Antibodies		
Rat monoclonal Ly6C-FITC (clone AL-21)	BD Pharmingen	Cat#553104; RRID AB_394628
Rat monoclonal CD11b-APC-Cy7(clone M1/70)	BD Pharmingen	Cat#557657; RRID AB_396772
Hamster monoclonal CD11c-PE-Cy7(clone HL3)	BD Pharmingen	Cat#561022; RRID AB_647251
Mouse monoclonal CD45.1-FITC (clone A20)	BD Pharmingen	Cat#553775; RRID AB_10926208
Mouse monoclonal CD45.2-APC (clone 104)	BD Pharmingen	Cat#558702; RRID AB_1645215
Rat monoclonal CD19-PE (clone 1D3)	BD Pharmingen	Cat#561736; RRID AB_395050
Hamster monoclonal CD3e-PE-Cy7(clone 145-2C11)	BD Pharmingen	Cat#552774; RRID AB_394460
Hamster monoclonal TCR-B-APC (clone H57-597)	BD Pharmingen	Cat#553174; RRID AB_398534
Rat monoclonal CD4-BV510(clone RM4-5)	BD Pharmingen	Cat#563106; RRID AB_2687550
Rat monoclonal CD8a-APC-Cy7(clone 53-6.7)	BD Pharmingen	Cat#561967; RRID AB_396769
7-AAD	BD Pharmingen	Cat#559925; RRID AB_2869266
Mouse monoclonal CD45R/B220-PerCP (clone RA3-6B2)	BD Pharmingen	Cat#553093; RRID AB_394622
Mouse monoclonal NK1.1-PE (clone PK136)	BD Pharmingen	Cat#561046; RRID AB_396674
Rat monoclonal Ly6G-BV510(clone 1A8)	Biolegend	Cat#127633; RRID AB_2562937
Rat monoclonal CD45-BV421(clone 30-F11)	Biolegend	Cat#103133; RRID AB_10899570
Rat monoclonal TLR4-APC (clone MTS510)	BioLegend	Cat#117601; RRID AB_313788
Rat monoclonal TLR4-PE (clona MTS510)	BD Pharminogen	Cat#558294; RRID AB_397073
Rat monoclonal CD14-PE-Cy7 (clone Sa14-2)	BioLegend	Cat#123316, RRID AB_10645329
Rat monoclonal Siglec H-APC (clone 551)	Biolegend	Cat#129611; RRID AB_10643574
American Hamster monoclonal Helios-PE (clone 22F6)	Biolegend	Cat#137206; RRID AB_10552903
Mouse monoclonal CX3CR1-BV421(clone SA011F11)	Biolegend	Cat#149023; RRID AB_2565706
Rat monoclonal F4/80-PE (clone BM8)	eBioscience	Cat#53-4801-82; RRID AB_469915
Rat monoclonal FOXP3-PerCP (clone FJK-16s)	eBioscience	Cat#45-5773-82; RRID AB_914351
Fixable Viability Dye eFluor 780	eBioscience	Cat#65-0865-14; RRID AB_2869673
Anti-GAPDH	Proteintech	Cat#10494-1-AP
Anti-NR1H4/FXR	Cell Signaling	Cat#72105
Anti-NR0B2/SHP	ORIGENE	Cat#TA332442
Donkey Anti-Rabbit IgG, HRP-Linked Whole Ab	GE Healthcare	Cat#LNA934V/AG
Sheep Anti-Mouse IgG, HRP-Linked Whole Ab	GE Healthcare	Cat#LNA931V/AG
Chemicals, peptides, and recombinant proteins		
TAK-242	CHEMSCENE	Cat#CS-0408
Meglumine	LKT	Cat#M1826
Carbon tetrachloride (CCl_4)	Thermo Fisher Scientific	Cat#BMS2030INST
Olive oil	SAJ	Cat#23-0400-6
Collagenase A	SIGMA	Cat# C5138
Anti- mouse CD95	BD Pharmingen	Cat#554255
Histopaque	SIGMA	Cat#10771
HBSS	Nacalai	Cat#17460-15
Anti-FcR (Fc block)	BD Pharmingen	Cat#553142; RRID AB_394656
Brefeldin A	BD Pharmingen	Cat#555029
Ampicillin	SIGMA	Cat#A9518

(*Continued on next page*)

Continued

REAGENT or RESOURCE	SOURCE	IDENTIFIER
Neomycin	SIGMA	Cat#N1876
Vancomycin	SIGMA	Cat#861987
Metronidazole	SIGMA-Aldrich	Cat#M3761
GAM Agar, modified (Nissui)	NISSUI	Cat#05433
Polymyxin B	SIGMA	Cat#P0972
TE buffer	Thermo Fisher Scientific	Cat#12090015
RPMI 1640 medium	SIGMA	Cat#R8758
Chenodeoxycholic Acid	Cayman Chemical	Cat#10011286
7-oxo-LCA	Steraloids	Cat#C1600-000
Tauro-β-muricholic Acid	Cayman Chemical	Cat#20289
(Z)-Guggulsterone	Cayman Chemical	Cat#39025-23-5
M-CSF	Pepro Tech	Cat#315-02
DMEM	Thermo Fisher Scientific	Cat#11054-020
PBS	Thermo Fisher Scientific	Cat#14190144
Lipopolysaccharides	SIGMA	Cat#L3012
Critical commercial assays		
Type 4 collagen 7S fragment (Lumipulse®) kit	FUJIREBIO	Cat#20036
MMP2 Quantikine® ELISA kit	R&D Systems	Cat#MMP200
TIMP1 Quantikine® ELISA kit	R&D Systems	Cat#DTM100
HMGB1 ELISA kit	Arigo Biolaboratories	Cat#ARG81351
Soluble CD14 Quantikine® ELISA kit	R&D Systems	Cat#DC140
GPT/ALT-PIII assay	Fujifilm Japan	Cat#14A2X1004000010
In vivo MMP activity (MMPsense 680)	Perkin- Elmer	Cat#NEV10126
Intracellular Fixation & Permeabilization Buffer Set	Thermo Fisher	Cat#88-8824-00
RNeasy Micro Kit/RNeasy Mini Kit	QIAGEN	Cat#74106
iScript cDNA Synthesis Kit	Bio-Rad	Cat#1708891B04
SYBR Premix Ex Taq (Perfect Real Time) kit	TaKaRa	Cat#RR820A
Ex Taq Hot Start (TaKaRa)	TaKaRa	Cat#RR006A
AMPure XP (Beckman Coulter)	BECKMAN	Cat#A63881
Miseq Reagent Kit V3	Illumina	Cat#MS-102-3003
AMPure XP	BECKMAN	Cat#A63881
Chromium Single Cell 3′ Reagent Kit v2	10x Genomics	Cat#PN-120237
Deposited data		
scRNA seq	GEO; This paper	GEO: GSE189606
Experimental models: Cell lines		
Bone marrow-derived monocyte/macrophage, primary culture	Allen et al.[52]	N/A
Experimental models: Organisms/strains		
Mouse C57BL/6 [Specific-pathogen-free]	CLEA Japan	N/A
Mouse *Tlr4*$^{-/-}$ (C57BL/6 background)	Oriental BioService	RRID IMSR_OBS:4
Mouse C57BL/6NCr [Germ-free]	Sankyo Lab Service	N/A
Mouse C57BL/6 Ly5.1	Taconic Biosciences	N/A
Oligonucleotides		
Targeting sequences used in RT-PCR analysis, refer to Table S4	This paper	N/A

(*Continued on next page*)

Continued

REAGENT or RESOURCE	SOURCE	IDENTIFIER
16S rRNA 27F for 5′-AGAGTTTGATCCTGGCTCAG-3′	Cai et al.[53]	N/A
16S rRNA 1492R rev 5′-GGTTACCTTGTTACGACTT-3′	Cai et al.[53]	N/A
Software and algorithms		
Flowjo v10.7.1	Flowjo	https://www.flowjo.com/
GraphPad Prism 9	GraphPad	https://www.graphpad.com/
ImageJ	ImageJ	https://imagej.nih.gov/ij/
R version 3.6.1	The R Project	https://www.r-project.org
R scripts	Nakamoto et al.[54]	https://github.com/
QIIME2 software package version 2019.10	Nakamoto et al.[54]	https://qiime2.org
Prokka version 1.14.6	Seemann[55]	https://github.com/tseemann/prokka
BlastKOALA	Kanehisa et al.[56]	https://www.kegg.jp/blastkoala/
Other		
Methionine−choline-deficient (MCD) diet	Research Diets	A02082002BR
CE-2 diet (Normal chow)	Japan CLEA	N/A

RESOURCE AVAILABILITY

Lead contact

Further information and requests for resources and reagents should be directed to and will be fulfilled by the lead contact, Takanori Kanai (takagast@z2.keio.jp).

Materials availability

This study did not generate new unique reagents.

Data and code availability

Single-cell RNA-seq data have been deposited at GEO and are publicly available as of the date of publication. Accession numbers are listed in the key resources table. This paper does not report original code. Any additional information required to reanalyze the data reported in this paper is available from the lead contact upon request.

EXPERIMENTAL MODEL AND SUBJECT DETAILS

Patients

The analyses regarding human subjects were parts of an observational study approved before we started, by the institutional review board of Keio University School of Medicine (No. 20140177), according to the guidelines of the 1975 Declaration of Helsinki (2008 revision). Recruited study subjects provided prior written informed consents, which included blood sampling, study participation and analysis of clinical data. All of the study subjects received standard of care and treatment, according to their clinical presentation. Twenty-three patients with CHC treated by interferon-free direct-acting agents (DAAs) and achieved sustained virological response (SVR) indicative of successful viral eradication, were recruited. Peripheral blood samples were collected and maintained at -80°C at timepoints shown in Figure 9A. According to the dynamics of type IV collagen 7S fragment (4COL7S), a non-invasive serological fibrosis marker, and mechanistic ECM remodeling markers inclusive of MMP2 and TIMP1, patients were classified as early resolving (ER), delayed resolving (DR) and non-resolving (NR) groups of liver fibrosis resolution. In brief, according to the dynamics of 4COL7S, a phenotype of decreasing trends at both end-of-treatment (EOT) and SVR12w was classified as ER, while that of decreasing trends at EOT but not at SVR12 as DR. A phenotype of increasing trends at EOT and non-decreasing thereafter was classified as NR. Background characteristics were shown in Table S3. Six healthy donors (HD, four females and 2 males, aged 32 to 55 years) were also included in some analyses.

In vivo animal studies

C57BL/6 wild-type (WT; Ly5.2) mice were purchased from CLEA Japan (Tokyo, Japan) and *Tlr4*-knockout (*Tlr4*$^{-/-}$) mice (C57BL/6 background; Ly5.2) from ORIENTAL BioService (Kyoto, Japan). Wild-type littermates of *Tlr4*$^{-/-}$ mice were not utilized. Mice were maintained under specific pathogen-free conditions with a 12h dark/light cycle, unless specified. Age- and sex-matched WT Ly5.1 mice were purchased from Taconic Biosciences (Hudson, NY, USA)) and were utilized for bone marrow transplantation experiments. They were maintained at a temperature of 22–25°C and a relative humidity of 45–55%. Male germ-free (GF) mice (C57BL/6 background strain, 6–8-weeks old) were purchased from Sankyo Lab Service Corporation and were housed in the GF Facility of Keio University School of Medicine. Methionine−choline-deficient (MCD) diets were purchased from Research Diets (A02082002BR). Experiments were performed with male mice aged 8–12 weeks. No mice died in any experimental treatment or manipulation. All study protocols comply with institutional guidelines congruent to the Animal Research: Reporting of *In Vivo* Experiments (ARRIVE) guidelines. For sample size, see corresponding figure legends.

Primary cultures

BMDMs and iv vitro analysis

BMDMs derived from WT or age- and sex-matched *Tlr4*$^{-/-}$ mice and WT primary murine hepatocyte debris were prepared accordingly to previous reports.[8,52] Briefly, BM cells were isolated and cultured with M-CSF (at 10^4 U/mL; Pepro Tech, Cranbury, NJ, USA) containing DMEM (Thermo Fisher Scientific) supplemented with 10 % FCS, 1 % L -glutamine, 1 % sodium pyruvate, 1 % nonessential amino acids, and 1 % penicillin/streptomycin for 7 days at 37°C with 5% (vol/vol) CO_2. BMDMs were harvested, and 2 × 10^5 cells were seeded per well in 12-well plates, followed by the addition of 5 × 10^5 washed hepatocyte debris or control medium. The cells were cultured for another 16 h. Where stated, TAK-242 or meglumine control was added to the plated BMDMs 1 h before and maintained throughout the 16 h incubation with hepatocyte debris. Non-ingested hepatocytes were removed by vigorously washing thrice with PBS, and residual adherent macrophages were used for analysis. In some experiments, lipopolysaccharides (LPS; from *E. coli* B5, Sigma) were used for stimulation at a concentration of 1μg/mL for 4 h, or chenodeoxycholic acid (CDCA; from Cayman Chemical), 7-oxo-Lithocholic acid (7-oxo-LCA; from Steraloids), or Tauro-β-muricholic acid (TβMCA; from Cayman Chemical) were added at indicated concentrations 1 h following the addition of hepatocyte debris. (Z)-guggulsterone (GS; from Cayman Chemical) at a concentration of 20 μM added 1 h before 7-oxo-LCA was used for FXR antagonism.

METHOD DETAILS

Quantification of serum proteins

Measurements of serum levels of 4COL7S were clinically approved and available with commercial kits in Japan. In brief, 4COL7S was quantified using chemiluminescent enzyme immunoassay methods (reference level for normal adult, below 4.4 ng/mL). MMP2 (R&D systems, Minneapolis, MN, USA), TIMP-1 (Enzo Biochem, New York, NY, USA), HMGB1 (Arigo Biolaboratories), and sCD14 (R&D) via enzyme-linked immunosorbent assays (ELISA).

CCl_4 -induced liver fibrosis resolution model

Liver fibrosis was induced by injecting CCl_4 diluted in olive oil (1:9) (Sigma) intraperitoneally (0.6 μL/g body weight; Sigma) thrice per week for four weeks unless specified otherwise. Animals were examined at stated timepoints after the final CCl_4 injection till 96 h, as demonstrated in a previous study.[8] The results demonstrated in this previous study were utilized for sample size estimation.

MCD diet-induced liver fibrosis resolution model

Steatohepatitis with liver fibrosis was induced by 5 weeks of methionine−choline-deficient (MCD) diet (Research Diets, Cat# A02082002BR). The diets were then switched to normal diet (ND; CE-2 diet from Japan CLEA) for 10 days to induce spontaneous resolution.

TLR4 signaling inhibition

TAK-242 (Cayman Chemical, Ann Arbor, MI) was dissolved in meglumine (Sigma) for intravenous administration via tail veins at 10 mg/mL/kg. All mice tolerated the intravenous administration of TAK-242 well. For *in vitro* experiments, BMDMs were pretreated with TAK-242 or meglumine control at a concentration of 1 μM as reported.[57]

Assessment of liver injury and fibrosis

The livers were excised, fixed in 10% formalin, and embedded in paraffin. Serum alanine aminotransferase (ALT) levels were measured using a chemiluminescence method (Fujifilm, Tokyo, Japan). Hepatic extracellular matrix levels were evaluated by Sirius red staining and Masson trichrome staining of paraffin-embedded sections. Sirius red or Masson trichrome positive areas were quantified in five non-overlapping random fields (magnification × 200) on each slide using imaging software ImageJ (NIH, Bethesda, MD, USA). Hepatic hydroxyproline content was measured by high-performance-liquid chromatography (HP-LC; SRL Laboratory, Tokyo, Japan); values were expressed as μg hydroxyproline/g of liver tissue.

Hepatocyte debris preparation

Isolation of hepatocyte was done accordingly to a previous report.[58] Livers were dissociated by collagenase-pronase perfusion and hepatocytes were isolated by density gradient centrifugation. After washed for three times, isolated hepatocytes were cultured overnight at 37°C 5% CO_2 on collagen-coated tissue culture flasks (Sigma) in DMEM (Thermo Fisher Scientific) supplemented with 10% FCS and 1% Penicillin/Streptomycin solution. Adherent viable hepatocytes were detached using trypsin, washed, and cultured in suspension in DMEM containing anti-mouse CD95 (1/500 dilution; Clone Jo-2; BD Pharmingen) at 37°C for 8 h for preparation of hepatocyte debris.

Isolation of liver NPCs

Liver nonparenchymal mononuclear cells were isolated from the liver accordingly to a previous report.[59] Livers were perfused through the portal vein with phosphate-buffered saline, minced, and passed through 100-μm nylon meshes. The filtrate was centrifuged at 50 × *g* for 1 min, and the supernatant was washed once. Cells were re-suspended in HBSS solution and overlaid on Histopaque solution (Sigma-Aldrich). After centrifugation at 780 × *g* for 20 min, liver mononuclear cells were collected from the upper phase of Histopaque.

Flow cytometry and FACS sorting

After blocking with anti-FcR (CD16/32, BD Biosciences) for 5 minutes, the cells were incubated with the specific fluorescence-labelled Ab at 4°C for 20 minutes. Relevant anti-rat isotype antibodies (BD Pharmingen) were used to assess background fluorescence. Cells for intracellular staining were fixed and permeabilized. Antibodies used in this study are shown in the key resources table. Lineage markers for exclusion were composed of NK1.1 and CD19, or CD3e as needed. Stained cells were analyzed using FACS Canto II (Becton Dickinson, NJ, USA), and the data were analyzed using FlowJo software (Tree Star Inc., Ashland, OR, USA). Cell sorting was performed using FACS Aria (BD), and over 95% purity of the sorted cells was confirmed.

In vivo MMP activity assay

To detect *in vivo* MMP activity, 2 nmol of MMPsense 680 (Perkin- Elmer) or vehicle control was administered at 72 h following the last injection of CCl_4 to mice via tail veins. Liver mononuclear cells were harvested at 96 h and analyzed according to the manufacturer's protocol. Liver mononuclear cells were identified using flow cytometry followed by identification of MMPsense-positive cells with excitation laser at 635 nm.

RNA extraction and RT-qPCR

Total RNA was extracted from cells using RNeasy Mini Kit or RNeasy Micro Kit (QIAGEN). Complementary DNA was synthesized by reverse transcription using the iScript cDNA Synthesis Kit (Bio-Rad). For quantitation, the following real-time PCR amplifications were performed in duplicate using the SYBR Premix Ex Taq (Perfect Real Time) kit (TaKaRa Bio, Ohtsu, Japan) with a Thermal Cycler Dice Real Time System (TaKaRa Bio). Pre-designed primers are shown in Table S3. Gene expression was calculated relative to 18S *rRNA*.

Single-cell RNA-seq analysis

Intrahepatic $CD11b^+$ $CD45^+$ cells (cell viability > 98%) were sorted from the pooled liver mononuclear cells of 5 mice (10,000 cells each) and loaded into Chromium Controller (10X Genomics, CA, USA). RNA libraries were then prepared using Chromium Single Cell 3′ Reagent Kit v2 according to the manufacturer's protocol (10X Genomics, CA, USA). The generated scRNA-seq libraries were sequenced using a 150 cycle (paired-end reads) with a HiSeqX (Illumina, CA, USA) and analyzed as previously reported.[60] Sequence reads from

all samples were processed by Cell Ranger (10X Genomics). The processed data were aggregated and analyzed by Seurat version 3.1.1.[61,62] Specifically, PCA analysis was performed to identify clusters, and 19 gene clusters (0-18) were projected on Uniform Manifold Approximation and Projection (UMAP) space with normalized gene expression. Subsequently, macrophage clusters (2-6) were identified via positive expression of *Lyz2* and *Cx3cr1* and negative expression of *Ncr1* (NK cells), *Cd3e* (T cells), and *Cd79a*, *Cd79b* and immunoglobulin genes (B cells) (Figures S3B and S3C). A gene expression heatmap showing an unbiased generation of the top ten differentially expressed genes for each cluster is presented in Figure 2D.

Gut sterilization

Mice were treated with a mixture of broad-spectrum antibiotics or drinking water, used as a control, via nasogastric tube (500 μL per mouse) at 48 h after the final CCl_4 injection. The following concentrations of antibiotics were used, as previously reported: ampicillin (6.7 g/L), neomycin (6.7 g/L), vancomycin (3.3 g/L), and metronidazole (6.7 g/L).[63] Our preliminary assessment (data not shown) and a previous report[64] revealed that large populations of bacteria were no longer detectable, and the total amount of bacterial genomic DNA was reduced remarkably following the administration of antibiotics.

16S rRNA metagenomic analysis

Mice were raised in the same facility but were not co-housed in the same cage. Fecal materials were collected at 24 h and 96 h after the last injection of CCl_4 on the same day and were analyzed accordingly to previous reports.[54,65] The hypervariable V3–V4 regions of the 16S rRNA gene were amplified using Ex Taq Hot Start (TaKaRa) and subsequently purified using AMPure XP (Beckman Coulter). Approximately equal amounts of each amplified DNA were then sequenced using the Miseq Reagent Kit V3 (600 cycle) and the Miseq sequencer (Illumina) according to the manufacturer's instructions. Sequences were analyzed using the QIIME2 software package version 2019.10 (https://qiime2.org). Forward and reverse reads were joined, denoised and chimera check using QIIME2 commands ("*qiime dada2 denoise-paired*"). Taxonomy was picked against *silva-132-99-nb-classifier.qza* (https://www.arb-silva.de/download/archive/qiime). Statistical analyses for alpha diversity metrics and generation of principal coordination analysis (PCoA) plots for beta diversity metrics were also done through QIIME2 commands (*qiime diversity* "*core-metrics-phylogenetic*", "*alpha-group-significance*", and "*beta-group-significance*"). Sampling depth (*–p-sampling-depth*) was set to the minimum number of remaining read counts among samples. PCoA was expressed by the qiime2R (v 0.99.13) and ggforce (v 0.3.1) packages in R software (v 3.6.1). Taxa-barplot was generated using R package qiime2R (v 0.99.13), phyloseq (v 1.30.0) and MicrobeR (v 0.3.2). The enriched bacteria in each group were identified by linear discriminant analysis (LDA) effect size (LEfSe); An LDA value >2 is considered significant. Correlation plot was generated using R package corrplot (v 0.84).

Metagenomic predictive functional profiling

Phylogenetic Investigation of Communities by Reconstruction of Unobserved States (PICRUSt2; https://github.com/picrust/picrust2/) was used with QIIME2 software package version 2019.10 (https://qiime2.org). The prediction of pathway abundance and EC abundance was used QIIME2 commands ("*qiime picrust2 full-pipeline*", "*qiime feature-table summarize*", and "*qiime diversity core-metrics*"). Sampling depth (*–p-sampling-depth*) was set to the minimum number of remaining read counts among samples.[66]

Isolation of *Erysipelotrichaceae* bacterium

Isolation of a specific bacterial strain from fecal material was done according to the method reported previously.[63] *Erysipelotrichaceae* bacterium was isolated from fecal samples of WT 96h mouse that were aseptically spread on GAM Agar, modified (Nissui) containing 50 mg/L Polymyxin B. The strain was cultured in an anaerobic chamber at 37°C for 48 h. 12 colonies were suspended in 1 mL of TE buffer and boiled for 10 min. After centrifugation at 9,000 g for 1 min, the supernatants were used as templates for PCR amplification. Amplification was performed in a 50 μL reaction mixture containing Ex Taq buffer, 0.2 mM of each dNTP, 1.25 units of Ex Taq HS (TaKaRa), 10 pmol of each universal forward primer 27F 5′-AGAGTTT GATCCTGGCTCAG-3′ and reverse primer 1492R 5′-GGTTACCTTGTTACGACTT-3′,[53] and 1 μL of template. After preincubation at 95°C for 3 min, 30 cycles consisting of 95°C for 30 sec, annealing at 55°C for 30 sec, and extension at 72°C for 1.5 min were performed, followed by a final extension step of 5 min at 72°C. PCR amplicons were purified using AMPure XP. The 16S rRNA was sequenced using BigDye

Terminator v3.1 Cycle Sequencing Kit and ABI PRISM 3130 Genetic Analyzer (Applied Biosystems). 50% of the colonies were *Allobaculum stercoricanis* DSM 13633 16S ribosomal RNA, partial sequence (94%).

Whole genome analysis

The sequencing library of *Erysipelotrichaceae* bacterium was sequenced on GridION X5 (Oxford Nanopore Technologies) and DNBSEQ-G400 (MGI TECH CO., LTD) using paired 200-bp reads. The genome was assembled by Unicycler (v0.4.8) (https://github.com/rrwick/Unicycler). Annotation of the assemblies were performed using Prokka (v 1.14.6).[55] Predict protein sequences were annotated against KEGG with BlastKOALA (https://www.kegg.jp/blastkoala/).[56]

Fecal material transplant

Fecal materials were collected at 24 h and 96 h after the last injection of CCl_4 and were stored at -80°C until use. The frozen stocks were thawed, re-suspended with vigorous shaking in 6-fold volumes of PBS and passed through a 70-μm cell strainer. CCl_4-treated GF mice were orally inoculated with 200 μL/time of the suspensions using a stainless-steel feeding needle, for three times, at 24, 48 and 72 hours after the last CCl_4 intraperitoneal injection.

Bone marrow transplantation

Partial BM chimeric mice were developed by shielding the liver before lethal irradiation (9.5 Gy) with a lead plate of 10-mm thickness to protect hepatic nonparenchymal cells accordingly to a previous report.[28] Total BM cells were harvested from the femurs and tibias of age- and sex-matched WT Ly5.1 mice (or *Tlr4*$^{-/-}$ Ly5.2 mice). Isolated BM cells were suspended in RPMI 1640 medium containing 10% fetal bovine serum and 2 mM EDTA and transplanted via the tail vein into irradiated recipient *Tlr4*$^{-/-}$ Ly5.2 mice (or WT Ly5.1 mice) at a dose of 6.0×10^6 cells. After 6 weeks, chimerism was confirmed via the analysis of peripheral blood myeloid cells.

Western blot analysis

Freshly harvested liver tissue was snap frozen with liquid nitrogen and stored at -80°C for protein extraction. 30 μg total cellular protein was subjected to analysis. After blocking with with TBS/0.05% Tween-20/5% skim milk, the membranes were probed with antibodies against GAPDH (dilution 1:10000), FXR (dilution 1:1000) and SHP (dilution 1:10000). After reaction with a secondary antibody, chemiluminescence was detected with ChemiDoc Imaging System (Bio-Rad).

Bile acid quantification

Fecal material or serum of the portal vein was collected at specific intervals after the last injection of CCl_4. BA concentrations were determined as reported by Honda et al.[67] Briefly, the feces were solubilized in 5% KOH/water at 80°C for 20 min; this heating step was omitted for portal vein serum samples. After the addition of internal standards and 0.5 M potassium phosphate buffer (pH 7.4), BAs were extracted with Bond Elut C18 cartridges and quantified by LC-MS/MS. Chromatographic separation was performed using a Hypersil GOLD column (200 x 2.1 mm, 1.9 μm; Thermo Fisher Scientific) at 40°C. The mobile phase consisted of (A) 20 mM ammonium acetate buffer (pH 7.5)-acetonitrile-methanol (70:15:15, v/v/v) and (B) 20 mM ammonium acetate buffer (pH 7.5)-acetonitrile-methanol (30:35:35, v/v/v). The following gradient program was used at a flow rate of 150 μl/min: 0–50% B for 20 min, 50–100% B for 10 min, hold 100% B for 15 min, and re-equilibrate to 100% A for 10 min. Oxo- (dehydro-) and epi- (iso-) BAs were prepared by reduction or oxidation of known bile acids, and were quantified by LC-MS/MS, as elaborated in detail in a previous report.[68] According to a previous report,[69] hydrophobicity index was estimated and calculated.

QUANTIFICATION AND STATISTICAL ANALYSIS

Statistical analysis

Statistical analyses were performed using GraphPad Prism software version 9.0 (GraphPad). Data are expressed as the mean ± standard error of the mean (SEM). Statistical evaluation of two groups was performed using the unpaired Student's *t*-test or Mann–Whitney test if data were not normally distributed. Kruskal-Wallis analysis for multiple group comparison. For post-hoc tests between groups, non-parametric Wilcoxon tests are applied. Spearman correlation was used for correlation analysis. Differences were considered statistically significant at $P < 0.05$.